5-2016

Assessment of Operating Condition Dependent Reliability Indices in Microgrids

Rafael Barreto de Medeiros
Clemson University, rafaelbarretodm@gmail.com

ASSESSMENT OF OPERATING CONDITION DEPENDENT RELIABILITY INDICES IN MICROGRIDS

A Thesis
Presented to
the Graduate School of
Clemson University

In Partial Fulfillment
of the Requirements for the Degree
Master of Science
Electrical Engineering

---

by
Rafael Barreto de Medeiros
May 2016

Accepted by:
Elham Makram, Committee Chair
Elham Makram
Keith Corzine
Richard Groff

ABSTRACT

Reliability analysis has been in place for decades, and its results are important for proper planning and operation of utility companies. Engineers must be able to quantify the current reliability of a system, as well as its potential improvement facing different modifications, in order to make informed planning decisions. Meanwhile, system operation has its performance measured through yearly reliability indices. The base of this method of analysis is the failure rate of the system components. In the traditional method, this probability of failure is determined by the components' manufacturer and is considered to be constant. However, it is reasonable to assume that the operation of the system has an effect on the likelihood of random failures to happen to the components. This study proposes a different modeling of failure rate, taking the system state variables into consideration. The probability of having system voltages or currents beyond the acceptable limits is added to the random probability of failure. With this new consideration, an IEEE test system has seven of its reliability indices quantified for comparison. The inclusion of the newly modeled failure rate lead to a worsening of 11.07% in the indices, on average. A second analysis is performed considering a third scenario, with PV and wind based micro sources present in the microgrid system, and an improvement of 0.71% on the indices is noticed, compared to the second scenario. Finally, the effects of storage systems in the microgrid are investigated through a fourth scenario, in which two 2MWh battery systems are introduced, and an improvement of 3.05% is noticed in the reliability indices.

ACKNOWLEDGMENTS

I would like to express my gratitude to Dr. Elham Makram, for her orientation during these two years, as an academic advisor and a professor. Our meetings were always able to lift my spirit and make me believe in myself.

I thank Dr. Keith Corzine and Dr. Richard Groff for accepting to be part of my committee, and especially for the great classes I took with each of them.

I would also like to thank the many friends I made in Clemson over the past couple of years, both colleagues in the department and outside. People who have made my experience here not only academically enriching but also very enjoyable personally. I hope these are people I can still be in contact with many years from now.

I express my appreciation to the Coordenação de Aperfeiçoamento de Pessoal de Nível Superior (CAPES), with the Ministry of Education of Brazil, through grant 88888.074885/2013-00, as well as for the support given to me by the Institute of International Education (IIE) and the Fulbright program.

Finally, I would like to thank my family back in Brazil, who I've missed very much, and who, despite the distance, has given me great support and orientation on the difficult parts of this journey.

TABLE OF CONTENTS

Table of Contents (Continued)

LIST OF TABLES

LIST OF FIGURES

List of Figures (Continued) Page

CHAPTER ONE

INTRODUCTION

The increasing demand for reliable electricity supply in developed countries, as well as the need to increase the reach of the power distribution system to underdeveloped countries, pushes the power industry to reinvent itself.

Following the growth of renewables, many customers are turning to distributed generation as primary, or complementary source of power. Microgrid systems are smaller scale versions of power distribution systems, which operate at a low distribution level voltage, and have several distributed energy resources (DER) [1] within it, such as solar panels, wind turbines, and thermal power plants. Electricity is, therefore, generated and consumed locally. These systems may operate connected to the main grid (on grid), or entirely independently (off grid).

The advantages of having smaller sized power distribution systems, such as microgrids, as opposed to the traditional concept of a larger and centralized system, with one single, or very few, points of generation, and a distribution system that radiates from them, is multifold. From the customer's point of view, the local supply of power improves the power quality of the grid, reduces emissions, as well as the cost sustained by the user. Given the smaller distance for transmission of power, these systems are more easily deployed in remote areas. From the electric utility point of view, microgrid implementation reduces the overall power flow, and consequently, the system losses, meaning less operational costs. Finally, a positive impact brought by these systems, and which is advantageous for both customer and utility, is related to the reliability of supply. For a

system with a central source of generation, any fault happening between the source and the load area would have a heavier impact than a fault happening in a loop connected microgrid with multiple sources of supply, in which demand could be rearranged between sources, for example.

One of the ways in which power companies have their performance evaluated is through the reliability of power supply experienced by its customers. It is expected of a reliable systems to be able to respond quickly and efficiently to faults, keeping customer disconnections to a minimum, both in quantities, as well as in duration. Billinton [2] demonstrates the standard analysis to quantify the reliability of supply of a distribution system. This method consists of determining the probability of failure (failure rate) of every element in the system, and for each of these possible faults, analyzing what load points have their supply cut off, and for what duration.

The traditional method of quantifying the reliability of a system through its reliability indices considers the failure rate of its components to be constant. This means that the probability that an element experiences a random fault is the same at all times, regardless of how the system is being operated. However, the current state of the distribution system's power flow should have an effect on the likelihood that one of its elements come to a fault. A section of a cable, for example, is more likely to come to a random failure if subjected to more intense currents over its lifespan.

Moreover, this study considers scenarios where the ANSI standards are exceeded to be faulted. Voltage limits are set by ANSI regulations, while current limits are set by the manufacturers of each component. The probability that the system power flow is such that

these limits are surpassed is taken into consideration, and adds to the system's failure rate. Xu [3] proposes a short term, hourly, reliability analysis, unlike the usual yearlong analysis carried out by utility companies. He also proposes the modeling of the system's failure rate as a function of its operating condition, and reaches the conclusion that the operating condition can affect both the frequency and the duration of interruptions. The probability of incorrect actions by the protection system is what is considered in this reference as responsible for the negative reliability impacts. This reference, however, doesn't consider the effects on reliability caused by random failure, for example. The concept of failure rate modeling presented is modified in Chapter 4 and applied to this study.

Once the reliability of the IEEE test system is quantified through a more traditional method of analysis, the proposed method of failure rate modeling is put into place for the same system, and results are compared. Given that an extra probability of failure is being considered for this second case, it is expected that the reliability indices will show a less reliable system. Given the local generation characteristic of a microgrid, the effect of Distributed Generation (DG) sources regarding reliability is also investigated. A first scenario without DG sources is compared to a second scenario in which they are introduced. Finally, the impacts brought by storage systems are quantified. Because of the weather dependent power delivery behavior of renewables, storage systems are often adopted in microgrids.

Organization of the Thesis

This thesis is organized as follows: Chapter 1 brought the introduction to the topic of reliability, and the characteristics of the traditional analysis. The modifications on this analysis, regarding failure rate modeling and its relevance, are explained.

Chapter 2 details both types of DER that are being considered in this study: solar photovoltaic (PV) and wind based generation. The chapter goes through the fundamentals of both these technologies, as well as its impacts on power system operation and reliability. The mathematical modeling of their power injection behavior, and their relation to meteorological conditions are presented, and the resulting equations will be used for subsequent analysis in the study.

The reliability assessment method presented in [2] is explained in further detail in Chapter 3, as an example feeder has its reliability indices calculated step by step for two different possibilities of protection arrangement. Chapter 3 also presents the IEEE test system, in which this basic analysis from [2] will be extended and applied. The resulting reliability indices from the test system are obtained, and will be used in the subsequent chapters as a basic, or standard, set of results. Different modifications for the reliability analysis will be proposed and those results will serve as ground for comparison.

Chapter 4 introduces the Back/Forward sweep method, which is the numerical power flow method used to describe the microgrid. The modeling of failure rate as a function of the resulting variables from power flow analysis is detailed. This modeling of failure rate will work as a link between power flow and reliability analysis. Finally, the resulting indices calculated hourly for a one year period are plotted at the end of the chapter.

Three scenarios are compared: the first set of results come from the standard method of reliability analysis, with constant failure rate. These results are, therefore, constants. The second set of results consider the proposed modeling of failure rate and, thus, vary throughout the year as the system's power flow varies. The third and final set of results in this chapter compares the effect of the introduction of DG sources in the microgrid.

Chapter 5 brings a final analysis, similar to those performed in Chapter 4, but regarding the effects of storage systems. The different possible placements of the battery systems are discussed and the resulting indices are compared.

Chapter 6 brings the conclusions of the study, as well as points out possible improvements for future works.

CHAPTER TWO

CONCEPTS OF RENEWABLE ENERGY

With the environmental impacts of human activity becoming more evident and undeniable, the alternative for power system operations is shown to be the reduction of greenhouse gas emissions [4]. Sources of electricity generation based on renewable primary sources are not yet playing such a major role in power supply worldwide, when compared to more traditional technologies such as coal, or natural gas based thermal generation.

However, given the increased awareness regarding global warming, as well as the expectation that the global market will face a shortage of fossil fuel supply sometime within this century [5], the absolute growth of "clean" energy generation has been remarkable over the last decade, and is expected to be even more accelerated in the near future. Some authors give more conservative predictions, such as the World Energy Council, which envisages that, by 2050, the global energy mix will be made up of at least eight energy sources (coal, oil, gas, nuclear, hydro, biomass, wind and solar), with none of them expected to have more than a 30% share of the market [6]. On the other hand, works have been showing an even deeper participation of renewables such as wind and solar, with special remark to the latter. In [7], for example, the worldwide statistical growth of solar photovoltaic is analyzed, and a conclusion is drawn that, if investments in research and development are maintained, this technology may be responsible for supplying the totality of power demanded on earth. Either way, it is clear that the study of these technologies is promising and important to the future of power systems.

Two different types of renewable power generation were approached in this work: Wind based and solar PV based. The theoretical aspects of both of these technologies, as well as their mathematical modeling are explained in this chapter.

Wind Generation

Air masses are moved around the planet due to its shape, the slope of its axis relatively to the sun, its movements of rotation and translation, and above all, the different temperatures on its surface [8]. Solar irradiation is stronger in the tropical regions than in Polar Regions. For that reason, air around the equator line is warmer and has lower density, while polar air is colder and denser, and there tends to be a natural exchange of air masses between these regions.

The kinetic energy of the air masses is converted to electricity through wind generators, such as those shown in Figure 2.1 [9]. The available energy is proportional to the air mass, as well as its speed. Given that the mass is depending on factors as the global position and altitude that the wind generator is going to be put to operation, those values are usually determined by the manufacturer and assimilated into constant values for the operation of the generator. Therefore, the power output of a generator is more directly affected by the changes in wind speed around it. For that reason, it is said that its power injection is largely weather dependent.

Figure 2.1 - Wind generators

Wind generators have controllers that respond to changes in wind velocity. Three velocity levels are determined by the manufacturer for a specific generator model: cut-in speed, nominal speed, and cut-out speed. For wind velocities of less than the nominal value, the generator's control will try to maximize the power absorbed from the wind by controlling the machine's torque. For cases with very low wind speeds, below cut-in value, the system is not able to convert any energy, and the power output is brought to zero.

On the other hand, for wind velocities higher than nominal value, the angle between the generator's blades and the wind speed vector is adjusted by the controller, such that the power delivered is constant and at nominal value, as well as minimizing mechanical stresses, assuring that there won't be any damages to the turbine. For cases with too high wind speeds, above cut-out speed, the controller will protect the blades and the power delivery will, again, be brought down to zero.

The mathematical modeling of these wind generators can be done in different levels of detail. This research aims to observe the effects that the power injected by these

sources has in a micro grid, and therefore only the power output, and its relation to weather conditions, i.e., wind speed are relevant. The equations that relate power injection (Gw) and wind speed (V) are shown below [3].

$$G_W = \begin{cases} G_{RATE}, & V_{RATE} \le V < V_{co} \\ \dfrac{G_{RATE}(V - V_{ci})}{V_{RATE} - V_{ci}}, & V_{ci} \le V < V_{RATE} \\ 0, & otherwise \end{cases} \quad 2.1$$

Where G_{RATE} is the nominal power determined by the manufacturer. V_{ci}, V_{RATE}, and V_{co} are the cut-in wind speed, nominal wind speed, and cut-out nominal speed, respectively.

Different regions of the planet are more or less fit to have wind generation explored, given the considerable variation in wind speed. Figure 2.2 [10] shows the resulting mean values of wind speed for different regions of the United States, for measurements taken during December 2015. From that figure, the Northwest coast, the Midwest region, as well as the state of Florida seem to show better wind profiles than other areas of the country. However, to plan the expansion of wind generation, it necessary to pursue much longer and much more detailed studies. The results showed in Figure 2.2 are not enough to jump into any sort of conclusion. It is possible that some of those regions have a steadier profile of wind speed, while others have stronger winds during a certain part of the day, and barely any during the remaining hours.

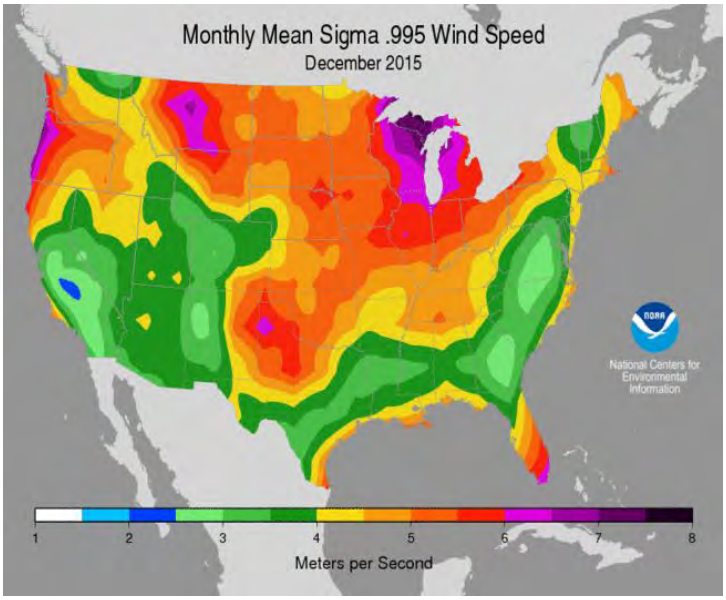

Figure 2.2 – Different mean wind speed values across the country

To illustrate how wind velocity might change during a one day period, Figure 2.3 [11] shows the wind speed profile for the first day of each season, during the year of 2015, in the city of Clemson, SC. The four profiles are from March 20th, June 21st, September 22nd, and December 21st, from top to bottom. Those are the first days of spring, summer, fall and winter seasons of 2015, respectively. The figure shows how much wind profile changes across the year for this region. The first plot, for example, shows relatively high wind speed during the night, while a good portion of the day has almost no wind. The last plot, on the other hand, shows a relatively firm wind during the day, and lower velocities during the night.

The variation between two consecutive days, as well as between years is also evident. This unpredictable characteristic of this power source shows to be a hurdle in its increasing penetration.

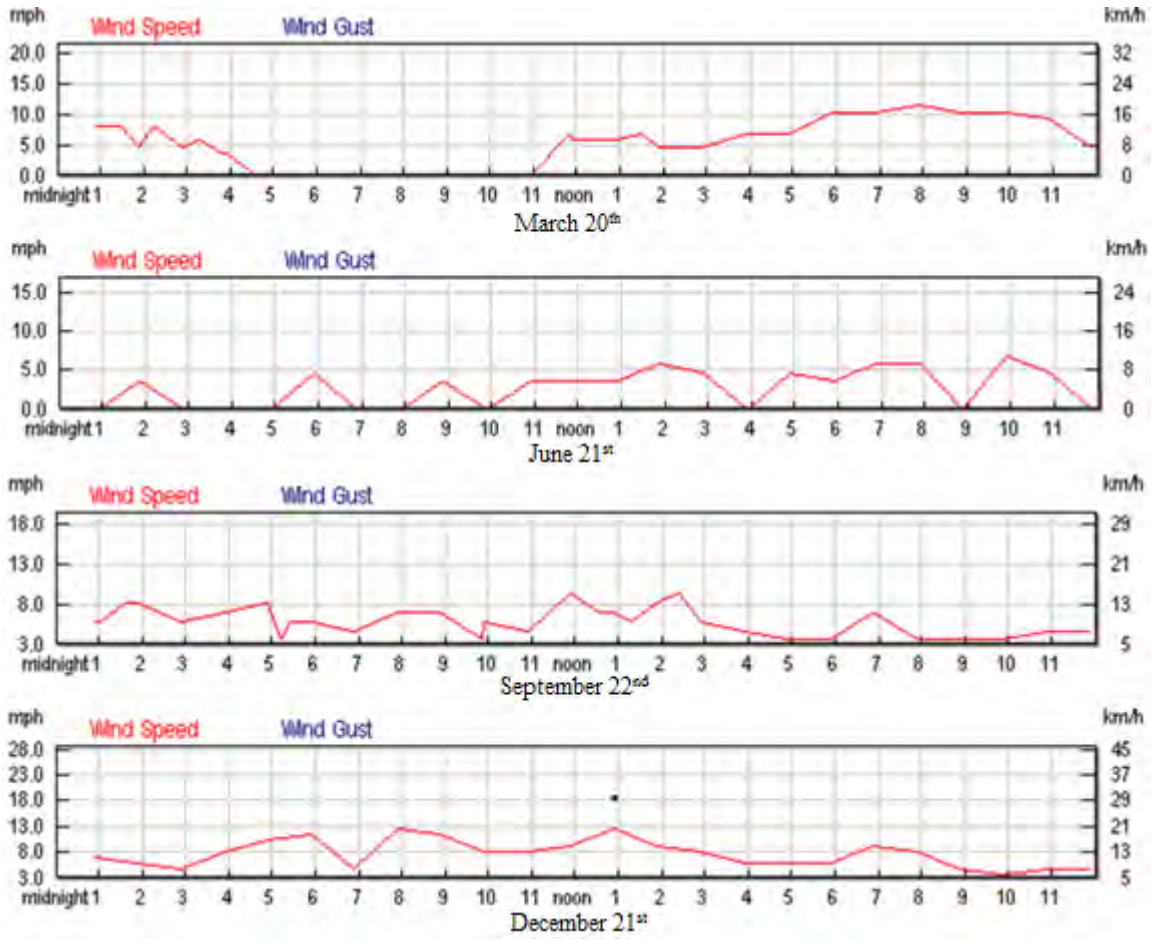

Figure 2.3 – Daily wind speed profile for different seasons in Clemson, SC

Solar Generation

The photovoltaic effect was discovered in 1839 by French physicist Edmond Becquerel [12]. It was found that some materials produce small amounts of DC electric current when exposed to sunlight. That technology had little commercial application at first, when energy conversion between solar irradiance and electricity was done with around 1% to 2% efficiency, and new materials were tested. Between the 1940s and 1950s, when the first crystalline photovoltaic solar cells were being produced with an efficiency

of 4%, this technology started to be envisioned for space applications, such as the powering of commercial satellites.

In the 1970s, rising energy costs, sparked by a world oil crisis, renewed interest in making PV technology more affordable. Since then, the federal government, industry and research organizations have invested hundreds of millions of dollars in research, development and production [12], making this technology economically competitive.

For a certain semiconductor material, there is an amount of energy called "band-gap", which indicates how much energy must be provided to the atom in order to move an electron from the valence band to the conduction band, freeing it from atomic bond in order to produce electric current. Sunlight is composed of photons, which can be seen as packets of solar energy. When a photon of sufficient energy strikes the material, it frees an electron from its connection with its respective atom, creating both an available negative charge, and positive charge, with the latter being the "hole" where that electron once resided. The movement of both these particles across the material is what will constitute electric current.

In order to move these electric charged particles, an electric field must be created. The most common way to make that happen is to dope the semiconductor material that is being used in the process. Assuming that material to be silicon, which is by far the most used semiconductor material for manufacturing of PV cells, then that material would be usually doped with atoms of Phosphorus and Boron.

Silicon has 4 valence electrons. For the doping process, a layer of phosphorus, which has 5 valence electrons, is applied to the silicon and heated, in order for its atoms to diffuse into the silicon. Once the temperature is lowered, 4 of the Phosphorus electrons will

replace the bonds with Silicon atoms, while one of them will be left as a permanent valence electron. This material will be considered “n-type”, given that it has what can be seen as an excess of negative charges. Similarly, once Silicon is doped with Boron, which has only 3 valence electrons, the resulting material will be called “p-type”, and will have an excess of positive charges.

Once both these materials are put together, an electric field forms at the junction (known as p-n junction). That electric field is what will push the electrons, once they receive enough energy from the solar photons, through the p-type material, and into the external electric circuit that must be connected in order to conduct the electric current.

Solar cells can be connected in series or in parallel, in order to achieve considerable levels of power delivered, as well as the desired level of voltage. In the series connection, the cells have the same magnitude of current circulating through all of them, and their voltage levels are added. As for the parallel connection, the voltage level is the same, and all cells contribute to a larger amount of current injected. The set of series or parallel connected cells is called a PV module, the connection of multiple modules is called a panel, and the connection of multiple panels is called an array.

The operation curve of a solar cell is illustrated in Figures 2.4 and 2.5. Figure 2.4 shows the relation between the current that the module is capable to deliver, and the voltage between its terminals. From that curve, it is possible to see that only one point of operation will deliver the maximum capacity of the cell, which is what is evidenced in Figure 2.5. Solar systems are connected to the power grid through DC-AC inverters, which are responsible not only for the conversion of power, but also for the tracking of this optimal

point. The system would, therefore, oscillate around the peak point of the plot in Figure 2.5. This control is known as Maximum Power Point Tracking, or MPPT.

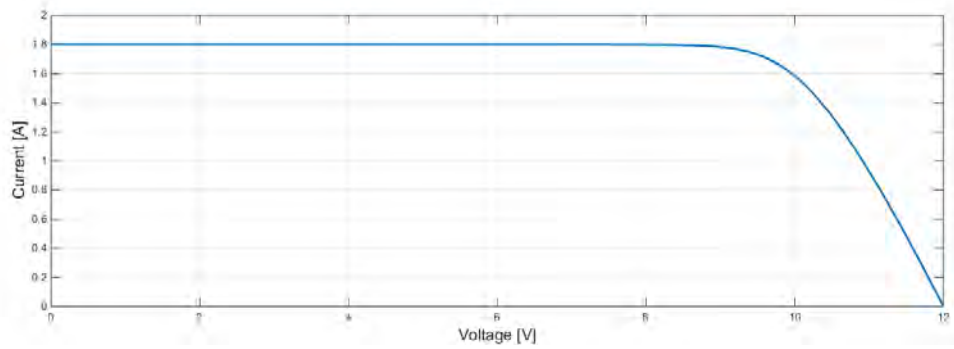

Figure 2.4 – Current versus voltage characteristic of a PV module

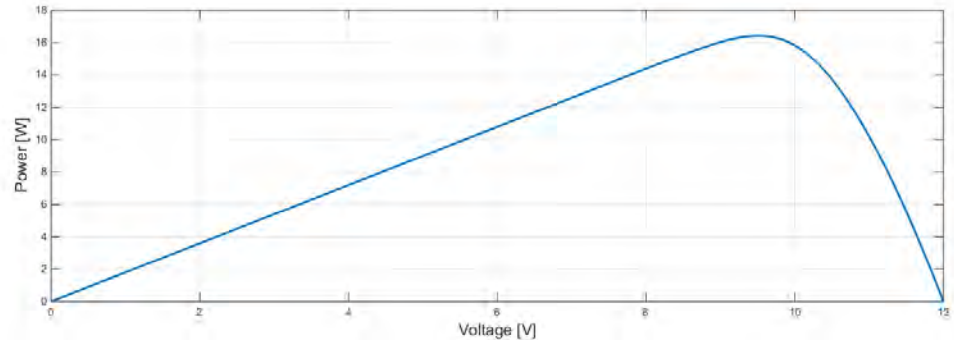

Figure 2.5 – Power versus voltage characteristic of a PV module

Two main factor influence the performance of a solar cell: temperature and solar radiation. In [13], a 180 W ZED fabric mono-crystalline PV solar panel is tested, and the effects of varying operating temperature, as well as solar radiation, are shown in figures 2.6 and 2.7. Figure 2.6 shows that different operating temperatures impact the cell's open circuit voltage, while having very little impact on its short circuit current. Overall, for higher temperatures, the open circuit voltage is reduced, as is the maximum power the cell is capable to provide, and its performance is said to be decreased. On the other hand, Figure

2.7 shows that solar radiation is more closely related to short circuit current than open circuit voltage. For higher levels of radiation, the cell receives more photons, and produces higher currents, delivering more power.

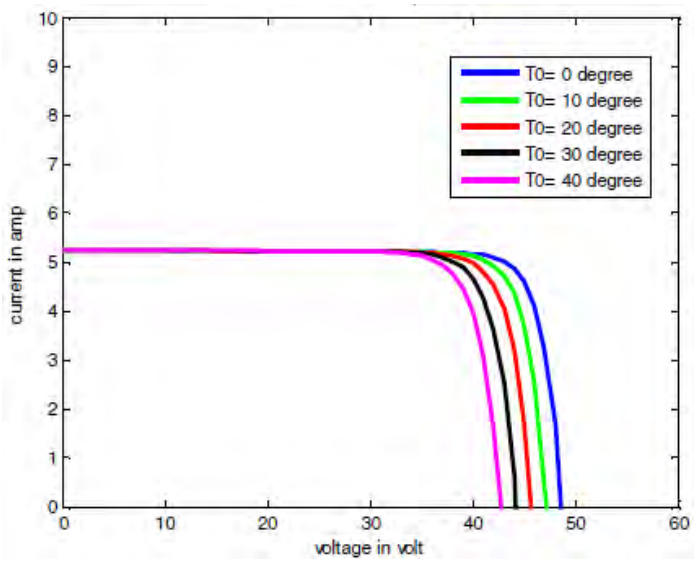

Figure 2.6 – I-V characteristics for variation of temperature and G=1000W/m2

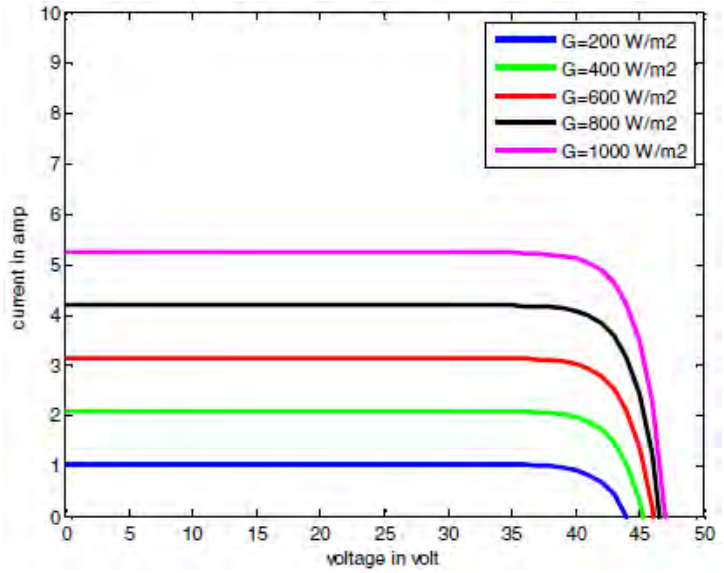

Figure 2.7 – I-V characteristics for radiation variation and T=30°C

The modeling of this behavior is necessary in order to consider these systems into the analysis proposed by this research. Similarly to what was presented for the wind based generation, equations are presented, in order to model the PV systems, and determine how they are dependent on the weather conditions. The equations that relate power injection (Gs) and temperature (V), as well as solar radiation (S) are shown below [3].

$$G_S = \frac{S}{S_{RATE}} \eta(E) \times G_{RATE} \qquad 2.2$$

$$\eta(E) = 1 - 0.0045 \times (E - E_{RATE}) \qquad 2.3$$

Where E_{RATE} and S_{RATE} are the rated temperature of operation and rated solar radiation, in which the manufacturer determines the cell's parameters and performance.

Given the weather dependence of this technology, the power injected by PV systems follows a curve similar to what is shown in Figure 2.8 [14]. This figure shows the solar irradiance, in W/m^2, measured by the National Energy Laboratory, in Oak Ridge, TN. The measurements were taken on a minute by minute basis, during the 5-day period of December 10th through 14th. Assuming there are no storage systems working in collaboration with these systems, power will be injected in peak intensity only during the few hours around 1pm (minute 780 in the plot), when radiation is peaking.

To illustrate how the two different DG technologies approached in this study perform during the day, the profile of wind speed measured in the same Oak Ridge, TN, area is showed in Figure 2.9 for comparison. It is clear that, for this region is particular, the wind speed profile is far more stable than the solar irradiance profile.

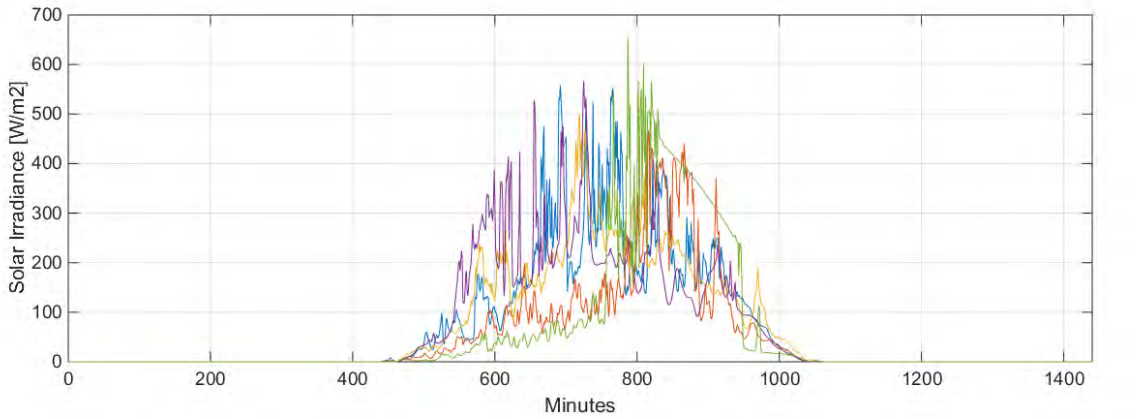

Figure 2.8 – Solar power daily profile

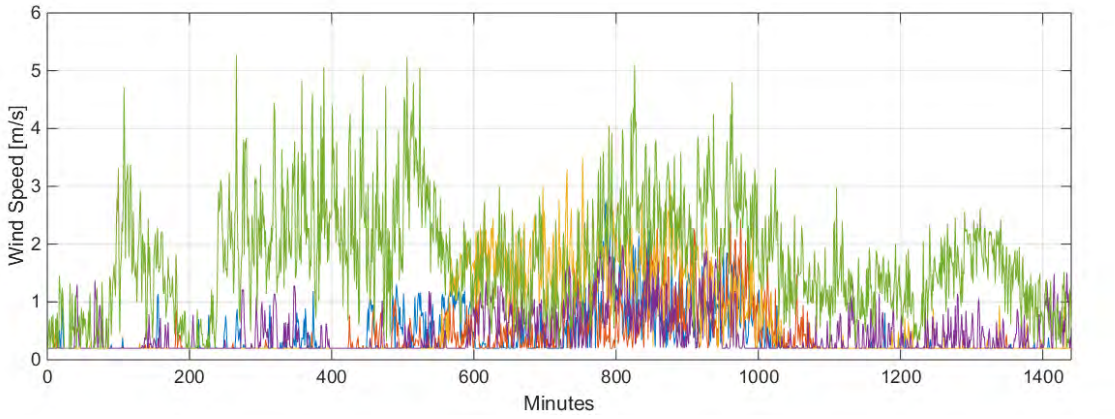

Figure 2.9 – Wind speed daily profile

The analysis performed in this study will consider different times of operation to an electric grid. Depending on the time of the day that is being analyzed, and their respective weather conditions, the renewable energy based sources of generation will perform accordingly, and the net load demanded will vary. Figure 2.10 [15] shows an example of load variation in the system supplied by California ISO, on January 11 of different years. Given the high penetration level of PV technology, the curve of the demanded load has a peculiar shape, called the “Duck Curve” [15].

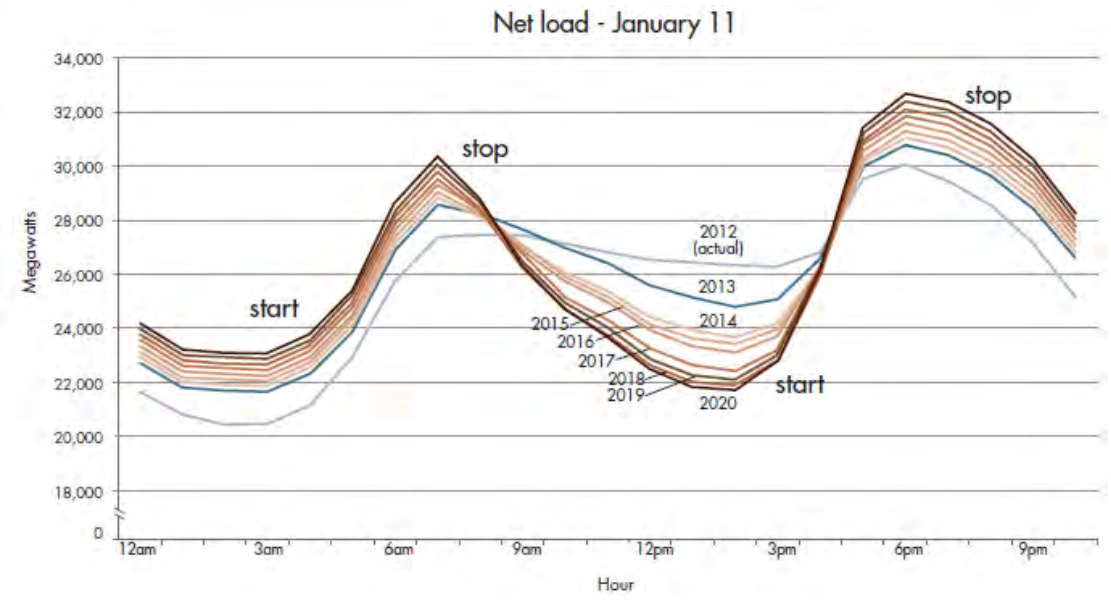

Figure 2.10 – The Duck Curve

It is shown on Figure 2.10 that the demanded load has a profile shape opposite to what was shown in Figure 2.8, given the high PV penetration. Around 7am, with sunset, the injection of PV based power stops the increasing demand of the morning, when customers are going about their morning routines, and creates this lower demand region, which is seen as the belly of the duck. At the end of the afternoon, around 4pm, when solar generation ends, the ISO must use other resources to meet the increasing load of peak hour, seen as the neck of the duck. If battery storage is introduced in the system, this resource can be used to reduce some of the high load demand of the end of the day.

In summary, this chapter presents the basic fundamentals of solar and wind based power generation. Figure 2.10 showed that PV generation has peak power injection during daily hours of high demand, which is interesting for the distribution system for reducing the maximum load. As for wind generators, its power input is depending on wind velocities,

which are usually more stable throughout the day, and might be higher during off peak hours. If that is the case, and high power injection happens during the night, battery storage might be an interesting solution to better use those resources during hours of higher demand. The modeling equations that relate the performance of both PV and wind technologies with the weather conditions have been presented, and will be used for the analysis done in following chapters.

CHAPTER THREE

RELIABILITY IN MICROGRID WITH RENEWABLE SOURCES

Reliability of electric supply is critically important for both the electric utility and the customers. Power outages occur mainly due to weather related events, such as strong winds, storms, snow or hurricanes, damaging overhead lines. These natural phenomena may cause damage to lines or poles, as well as cause trees or other objects to touch lines in the distribution system, producing short circuits.

Moreover, the elements that compose a distribution system are subjected to the possibility of failure at a certain point within its life span, just like any other product. Manufacturers of cables or transformers, for example, will perform statistical studies on samples of their products, and determine what is called the Failure Rate (λ) of their product. The Failure Rate is given as the number of faults per year that a certain component is, statistically, expected to fail. Since distribution systems are expected to be highly reliable, the Failure Rate of its components is usually very small, of the order of 0.01 failures/ year.

Considering a simple radial distribution system, composed of a set of elements connected in series, like cables, disconnects, transformers, busbars, etc., all elements between a certain point of supply and the source must be working in order for the loads connected to that point to be fed. If any of those elements fail, either by a random failure or by a weather related event, the load will be temporarily disconnected, and the reliability of supply will be compromised.

Distribution engineers are responsible for designing the systems such as to maximize efficiency. In face of multiple possibilities of investments and upgrades in a

distribution system, it is important that the engineers be capable of quantifying how reliable the system is at a certain point, and how much more reliable it would become, for each possible action, so to take an informed decision. In order to do so, reliability indices are created.

Reliability Indices

It is important to have in mind two basic concepts: first, Failure Rate (λ), as being the frequency with which system elements randomly fail. Second, Outage Time (U) as being the duration that an element is expected to be disabled after it experienced failure, and is given as:

$$U_i = \lambda_i \times r_i \qquad 3.1$$

Where "i" refers to the ith element of the system, and "r" means the repair time of that element, in hours. The repair time is determined by the utility and depends on how the protection scheme of the grid is set, how selective and how sensitive it is. With these concepts in mind, the reliability indices can be calculated, as shown below [2].

(i) System average interruption frequency index (SAIFI)

$$SAIFI = \frac{customer\ interruptions}{customers\ served} = \frac{\sum \lambda_i N_i}{\sum N_i} \quad \text{[interruptions/customer]} \qquad 3.2$$

Where N_i is the number of customers connected to loadpoint i.

(ii) System average interruption duration index (SAIDI)

$$SAIDI = \frac{total\ interruption\ duration}{customers\ served} = \frac{\sum U_i N_i}{\sum N_i} \quad \text{[hours/customer]} \qquad 3.3$$

(iii) Customer average interruption duration index (CAIDI)

$$CAIDI = \frac{total\ interruption\ duration}{customer\ interruptions} = \frac{\sum U_i N_i}{\sum \lambda_i N_i} \quad \text{[hours/customer]} \qquad 3.4$$

(iv) Average service availability index (ASAI)

$$ASAI = \frac{hours\ of\ available\ service}{hours\ demanded} = \frac{\sum N_i \times 8760 - \sum U_i N_i}{\sum N_i \times 8760} \qquad 3.5$$

(v) Average service unavailability index (ASUI)

$$ASUI = \frac{hours\ of\ unavailable\ service}{hours\ demanded} = \frac{\sum U_i N_i}{\sum N_i \times 8760} = 1 - ASAI \qquad 3.6$$

(vi) Energy not supplied index (ENS)

$$ENS = total\ energy\ not\ supplied\ by\ the\ system = \sum L_i U_i \quad \text{[kW.h]} \qquad 3.7$$

Where L_i is the average load connected to loadpoint i.

(vii) Average energy not supplied (AENS)

$$AENS = \frac{total\ energy\ not\ supplied}{number\ of\ customers\ served} = \frac{\sum L_i U_i}{\sum N_i} \quad \text{[kW.h/customer]} \qquad 3.8$$

Application to a Distribution Feeder

To understand how the quantitative reliability analysis discussed in 3.1 is applied to an actual distribution system, Figure 3.1 shows an example of a distribution feeder. This feeder, although simple, will have similar analysis to the one later performed to the test system adopted in this research.

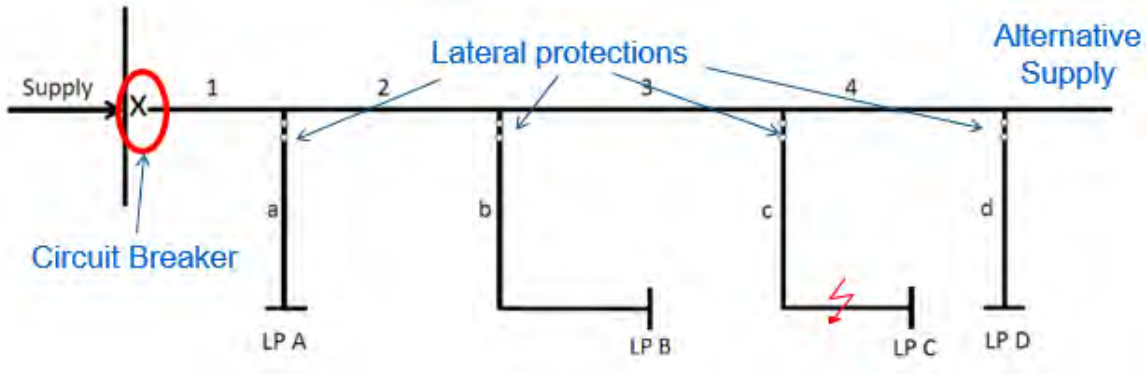

Figure 3.1 – Example of a distribution feeder

Many distribution systems are designed as single radial feeder systems. Others, designed as meshed systems, will have radial feeders operating normally, and connected through tie-lines, or normally open connectors. Those connectors offer the feeders the possibility that a feeder isolates a fault along its line, and rearranges the load beyond the faulted point to an alternative feeder, so that load doesn't have to be disconnected. That is represented in Figure 3.1 by the remaining cable section marked "Alternative Supply".

It was explained how the reliability of supply is a function of how often the elements in the system fail, i.e. their failure rates. The other aspect of which reliability will depend is how well organized the protection scheme is. To illustrate that, two analysis will be done on the feeder in Figure 3.1, for two different protection scenarios [2].

Table 3.1 shows arbitrary values of reliability parameters for each component of the feeder in Figure 3.1. Given that failure rate is usually given as a function of the cable's length, it is important to know the length of cables on the main, as well as on the lateral distributors. For this example, it is assumed that all sections in the main distributor have the same failure rate [failures/yr.km], as well as all the lateral distributors. Therefore, on Table 3.1, the sections with higher failure rate [failures/yr.] are simply being considered to be longer sections.

Component	λ (failures/yr.)	r (hours)
Main Section		
1	0.2	4
2	0.1	4
3	0.3	4
4	0.2	4
Lat. Distributor		
a	0.2	2
b	0.6	2
c	0.4	2
d	0.2	2

Table 3.1 – Reliability parameters for the feeder on Figure 3.1

First Scenario

First, assuming a very simplistic scenario, in which the protection scheme would be composed only by one main breaker on the head of the feeder, it is possible to predict that the reliability of supply for each loadpoint will be identical. For any fault, either at a

main or at a secondary section, the main breaker would be activated, and all loadpoints A through D would be disconnected.

The second step would be to perform an analysis of each loadpoint, to determine how long its load would be impacted for a fault happening on each section across the entire feeder. Table 3.2 shows an example of this analysis applied to loadpoint A.

Component failure	λ (f/km)	r (hours)	Unavailability (hours/yr.)
Main Section			
1	0.2	4	0.8
2	0.1	4	0.4
3	0.3	4	1.2
4	0.2	4	0.8
Lat. Distributor			
a	0.2	2	0.4
b	0.6	2	1.2
c	0.4	2	0.8
d	0.2	2	0.4
Total	2.2	2.73	6.0

Table 3.2 – Analysis of loadpoint A for the first scenario studied

It can be observed that, although loadpoint A is the one being analyzed, given the simplicity of the protection scheme, faults on secondaries b through d will equally affect it through the opening of the main circuit breaker. Later on, in the second scenario, a slightly more complex protection scheme will avoid that. As was stated, it is not necessary to go through all loadpoints, given that they will all return the same results.

Now that the fault frequency and the unavailability per year of each loadpoint is defined, it is possible to calculate the reliability indices presented in section 3.1. The details of the customer loads are necessary for that. Table 3.3 brings arbitrary values for the number of customers connected to each loadpoint, as well as their average power demand. Using those values, and the formulas from section 3.1, the indices are calculated and shown in Table 3.4.

Loadpoint	Customers	Avg. Load (kW)
A	1000	5000
B	800	4000
C	700	3000
D	500	2000

Table 3.3 – Customers and load connected to each loadpoint

SAIFI	2.2 Interruptions/customer.yr.
SAIDI	6.0 hours/customer.yr
CAIDI	2.73 hours/customer.interruption.
ASUI	0.000685
ASAI	0.999315
ENS	84.0 MWh/yr.
AENS	28.0 kWh/customer.yr.

Table 3.4 – Reliability indices for the first scenario studied

Second Scenario

The second scenario would consider a slightly more efficient protection scheme, to illustrate how the protection affects the reliability indices. An additional protection possibility would be to install fuses on the connection of each lateral distributor with the main distributor, as it is shown in Figure 3.1. In that case, for a fault in lateral c, for example, only its respective loadpoint C would be affected, and all other loadpoints would be unharmed. It is evident, from this logic, that the reliability indices will look better for this case. However, it is still necessary to quantify those improvements, in order to have a clear understanding of cost and benefit analysis, or to compare this possible upgrade in the system with other viable options.

Table 3.6 shows the analysis performed for each loadpoint, similar to what was done in Table 3.2. The difference is that, for this case, the loadpoints will be affected differently according to where the fault is located and, therefore, we cannot apply the same analysis to all of them. Notice from Table 3.6 that for the analysis of loadpoint C, for example, the supply for that loadpoint will be affected by faults on sections 1 through 4 in the main distributor, but only by faults on lateral distributor c. The reliability indices for this new scenario are calculated again following the same equations from section 3.1 and are shown in Table 3.5. The percentual improvement in the reliability indices is also shown as a comparison between the results from both studied scenarios.

		Improvement
SAIFI	1.15 Interruptions/customer.yr.	- 47.7 %
SAIDI	3.91 hours/customer.yr	- 34.8 %
CAIDI	3.39 hours/customer.interruption.	+ 24.1 %
ASUI	0.000446	- 34.9 %
ASAI	0.999554	+ 0.024 %
ENS	54.8 MWh/yr.	- 34.8 %
AENS	18.3 kWh/customer.yr.	- 34.6 %

Table 3.5 – Reliability indices for the second scenario studied

As was to be expected, most reliability indices show considerable improvement due to this simple upgrade in the protection setup. ASAI shows a much smaller improvement given the fact that is already very close to the maximum unity value. CAIDI is the only index showing worse results for the second scenario. This index shows, on average, how long each customer is left without power for an interruption in any component in the system. In the second scenario, secondary faults were being less relevant to the reliability of supply, given that they would be correctly isolated by the fuses, and its impacts minimizes. Faults on the primary distributor, however, were still equally considered between both scenarios. As was shown on Table 3.1, the repair time for those faults is larger than for secondary faults. For that reason, the average outage time per fault was bound to increase in the second scenario, although the overall reliability of the system was improved.

	Loadpoint A			Loadpoint B			Loadpoint C			Loadpoint D		
Component failure	λ (f/km)	r (hours)	Unavailability (hours/yr.)	λ (f/km)	r (hours)	Unavailability (hours/yr.)	λ (f/km)	r (hours)	Unavailability (hours/yr.)	λ (f/km)	r (hours)	Unavailability (hours/yr.)
Main Section												
1	0.2	4	0.8	0.2	4	0.8	0.2	4	0.8	0.2	4	0.8
2	0.1	4	0.4	0.1	4	0.4	0.1	4	0.4	0.1	4	0.4
3	0.3	4	1.2	0.3	4	1.2	0.3	4	1.2	0.3	4	1.2
4	0.2	4	0.8	0.2	4	0.8	0.2	4	0.8	0.2	4	0.8
Lat. Distributor												
a	0.2	2	0.4									
b				0.6	2	1.2						
c							0.4	2	0.8			
d										0.2	2	0.4
Total	1.0	3.6	3.6	1.4	3.14	4.4	1.2	3.33	4.0	1.0	3.6	3.6

Table 3.6 – Analysis of all loadpoints for the second scenario studied

In conclusion, it is in the interest of the distribution engineers to make use of multiple indices, rather than focus on only one, in order to have an exact and quantitative understanding of how the reliability is being affected. As was evidenced by the behavior of the CAIDI in the example feeder, the analysis of one single index might lead to erroneous conclusions.

Reliability Test System

Reference [16] presents an IEEE reliability test system developed for educational purposes. The proposed system is consisted of a 6 busbar 33 kV transmission test system, defined as the RBTS. In this system, two busbars (BUS 2 and BUS 4) were selected, and distribution systems were developed for each one of them. This research is focused on the 11 kV distribution system developed from BUS 4, which is shown in Figure 3.2.

This distribution system is composed of 7 feeders connected in a loop through normally open tie-lines. These connections give the possibility of alternative supply, as was explained through Figure 3.1. Figure 3.2 shows that the tie-lines connect feeders F1 and F7, feeders F3 and F4, as well as feeders F5, F6 and F7. The total number of nodes and loadpoints are 67 and 38, respectively.

All the system information demanded for the reliability analysis are provided in [16]. Also, the reference provides reliability results for different case studies, i.e. different protection schemes and considerations. The IEEE proposed system is large enough so that realistic and practical factors can be observed, but still small enough to allow students to apply analysis through hand calculations and check their results.

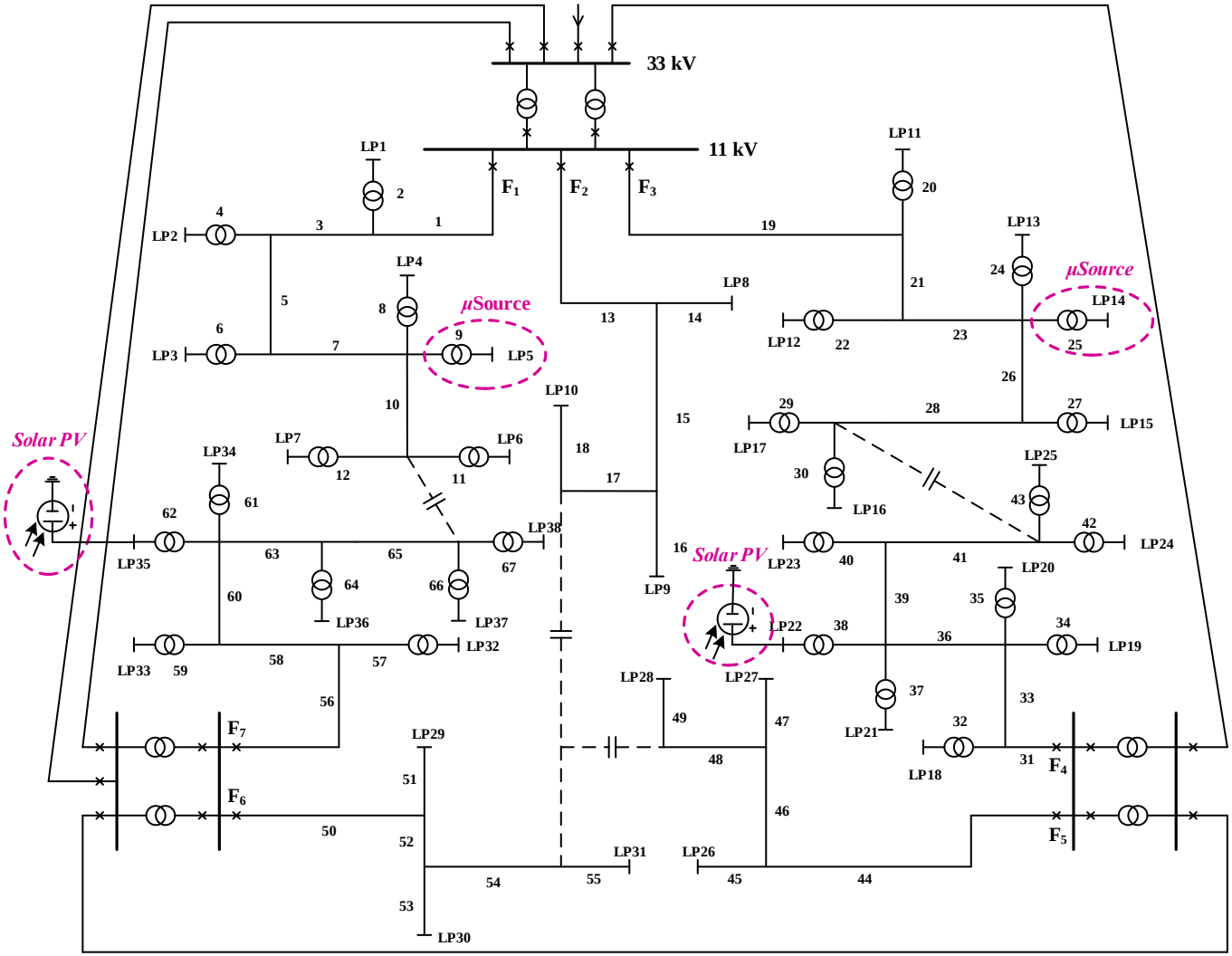

Figure 3.2 – IEEE 14-Bus test system

Figure 3.2 also shows the consideration of micro sources in the distribution system. Since microgrids are defined to be small scale power grids, with possible self-sufficient operation [17], Distributed Generation (DG) must be considered within. More specifically, two solar based utility scale DG sources, of nominal power 2.0 and 2.5 MW are connected to nodes 62 and 38, respectively, and two wind based DG sources, with nominal power of 2.0 and 3.0 MW are connected to nodes 25 and 9, respectively, as the figure shows.

As was addressed in chapter 2, both these DG sources are weather dependent. For that reason, their power delivery is not expected to be constant, and should vary according to factors as wind speed and solar illuminance. The analysis of this microgrid will be performed multiple times for different times of the day and, therefore, for different values of DG injected power, as will be explained later on Chapter 4.

The considerations made for this system are as follows: all feeders are considered to have one main breaker connecting it to the main source. Lateral distributors are protected by fuses. Disconnectors are present, and are capable to isolate any fault in the main distributor. Finally, for possible isolation of sections in the main distributor, all loads beyond the faulted point are transferred through the tie-line to an alternative feeder, as long as the second feeder is capable to handle the extra load.

In terms of failure rate, it is determined a constant value of 0.065 failures/yr.km on all feeders. The actual failure rate would have to take the lengths into consideration, and those can be consulted in [16]. The time of unavailability, or repair time, is of 0.5 hours for loads that are transferred between feeders, of 5 hours for loads that are disconnected after a fault on a cable, and of 200 hours for faults on a transformer.

The resulting reliability indices will be shown in Chapter 4, when a comparison between the results shown in [16] and those obtained through the analysis performed in that chapter will be made.

CHAPTER FOUR

FAILURE RATE MODELING AND RELIABILITY RESULTS

On the previous chapter, the concept of reliability of supply was explained, and the numerical analysis for the calculation of the reliability indices was described. In that analysis, the Failure Rate (λ) described the statistical frequency that distribution system components randomly fail. This value, determined by the manufacturers of such components, is considered to be a constant through the entire analysis. This chapter proposes a different approach on Failure Rate, considering it not only a simple constant, but a function of the actual state of its distribution system, described by a power flow study. A reliability analysis of the test system presented in Chapter 3 is then carried out, to evidence the difference in results between the standard analysis, presented in [16] and the one proposed in this study.

Back and Forward Sweep Method

In order to optimally operate existing power systems, as well as plan and design future expansions, it is fundamental to be able to calculate the voltages and currents in different parts of the system.

Commercial power systems are usually too large, so that hand calculations become too cumbersome. To address that problem, algorithms of numerical power flow analysis were developed. The main information obtained from these calculations are the magnitudes and phase angles of voltages at each bus, and the real and reactive power flowing in each

line [18]. From those, the state of the system is described, allowing protection studies, economical operation analysis, short circuit analysis, etc., to be carried out.

Power systems operate, most of the time, in steady state. Although small changes might occur, like switching actions, load changes and other transients, meaning that in a strict mathematical way, state variables are changing over time, it is still acceptable from an engineering point of view that a time-invariant model be used [19]. Transmission lines are represented through their π-model, which determines values of series impedance Z and line admittance Y. These values are processed though a determined algorithm and the calculations are numerically performed.

Generally, distribution networks are radial, and the R/X ratio is very high. For this reason, conventional Newton-Raphson and fast decoupled load-flow methods do not converge [20]. It was presented, in [20], a simple and effective method of running power flow analysis in a radial distribution system, which showed to be effective, and had a good simulation time, when compared to more traditional power flow algorithms. This method is called Back/Forward Sweep, and is illustrated by the flowchart shown in Figure 4.1. This was the method applied to the analysis of the test system presented in Chapter 3.

This power flow algorithm consists of several iterations starting from an initial guess of voltages and going between calculating new sets of voltages and currents in the system. Initially, the information will be read from the system model. A flat start of voltage, meaning voltages of magnitude of 1 pu and angle zero, is then assumed all across the system. The branch connections are analyzed in order to determine which branches are part of the main distributors and which ones feed final loadpoints. That is done so that the final

currents are defined beforehand, in what is shown in Figure 4.1 as step (i). This is done through the following equation:

$$I_i = \frac{S_{LOADi} + S_{DGi}}{V_i^*} \tag{4.1}$$

Where I_i is the current flowing into the loadpoint connected to node i. S_{LOADi} and S_{DGi} are the complex powers demanded by the loads and injected by the microsources, if there are any, in loadpoint i. V_i^* is the conjugate of the voltage in node i for the current iteration.

Once the currents in the final branches are determined, all others are determined upstream, simply considering current in node i to be the sum of all currents in nodes beyond i. That is referred to in the flowchart of Figure 4.1 as step (ii). With a new set of currents, a new set of voltages is obtained through equation 4.2, which will consist of step (iii) in Figure 4.1.

$$V(jr) = V(js) - I(jj) \times Z(jj) \tag{4.2}$$

The difference between the previous set of voltages and this one will be determined to be the error of the iteration, or step (iv) in Figure 4.1. A maximum error of 0.0001 pu was determined for the analysis of the test system. While the error is beyond that maximum value, the previous set of voltages will be updated, and the algorithm will perform step (i) again in a new iteration. Once the error is small enough, the final results are displayed.

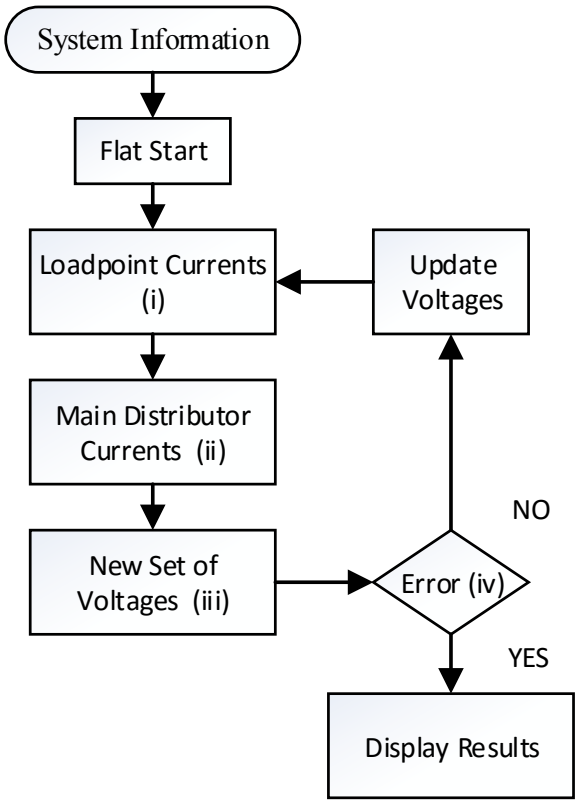

Figure 4.1 – Flowchart of the Back/Forward Sweep method

Failure Rate Modeling

A reliability study is usually performed on nominal conditions of operation. That means that a sample of components is put to a similar operation to what will be expected of it during its life span, and a statistical analysis of their mean time to failure is performed. However, in an actual distribution system, the conditions might not always be ideal, and components might be subjected to different values of voltage or current than what they were designed for. A cable that is subjected to a current beyond its nominal ratings, for example, is expected to have a higher probability of failure than if it were operating in ideal

conditions. For that reason, the non-compliance of the system's currents or voltages to their maximum or minimum values is also regarded as a failure in this study.

The American National Standards Institute (ANSI) determines limits for steady state voltage delivered to customers. Since the loads are always changing, it is impossible for the system to keep supply voltages always at nominal value. For this reason, ANSI establishes it to be acceptable for those voltages to vary between a minimum of 0.95 pu to a maximum of 1.05 pu [21]. As for currents, the maximum value that a component can withstand is determined by its manufacturer. The maximum current a component can be subjected to, in continuous operation, is called ampacity current. In transient operation, like in the case of a short circuit, those components can be subjected to even higher currents than the ampacity and still perform correctly, as long as the time of exposure is small enough.

State variables are a set of variables used to summarize the system's status. The state of a system, described by its state variables, is enough information to predict its future behavior, given that no external forces affect the system [22]. For the test system [16], its state variables are considered to be two: the set of system voltages, and the set of system currents. The state variables of the test system are, therefore, related to the probability of failure of its components.

Thus, a function between Failure Rate and state variables is proposed, working as a link between the power flow analysis and the reliability analysis, as is illustrated in Figure 4.2. The results of the power flow analysis, presented in section 4.1 will serve as input to the modeling, which will result in an updated value of Failure Rate, serving as input to the

reliability analysis, presented in Chapter 3 and, finally, resulting in quantifiable reliability, or reliability indices. This way, a more realistic result on reliability is expected to be achieved.

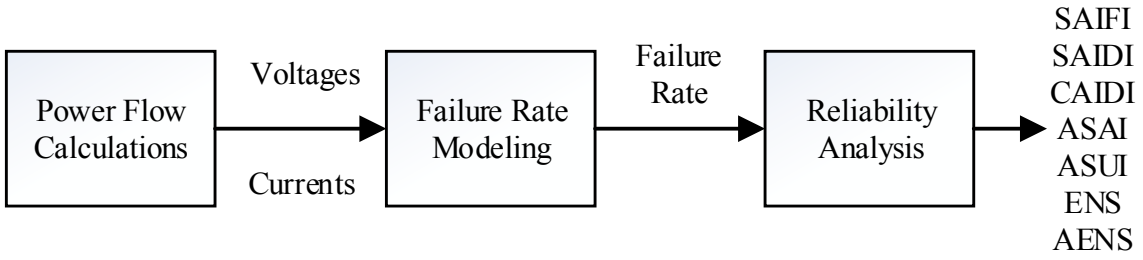

Figure 4.2 – Failure Rate Modeling

As was explained, the current state of the system's state variables might make it more likely for failures to occur, with failures being treated as random malfunctioning of elements, or simply the noncompliance of the limits established by the norm. That probability is additional to the standard probability of failure by the elements or, the standard failure determined by the manufacturers. That is represented through equation 4.3 [3], where $\lambda_t(x)$ is the failure rate with respect to the state variables (voltages and currents), during the analyzed interval Δt. λ_0 is the standard failure rate, which is determined to be 0.065 failures/km.yr [16], and $P_t(x)$ is the additional probability given by the current state variables for that period of time. Δt is a smaller interval of time to be analyzed. The reliability analysis will be performed for each of the 8760 hours within a one year period, as will be explained in more detail in the next topic.

$$\lambda_t(x) = \frac{P_t(x)}{\Delta t} + \lambda_0 \times \frac{\Delta t}{8760} \tag{4.3}$$

$P_t(x)$ is quantified by equation 4.4, where the integral element gives the cumulative distribution function of $f_t(x)$, between zero and x_s. For state variable x being either current values or voltage values, x_s represents the short term rating value, indicating the feeder's capability to handle short term operation following contingencies [3]. The difference between the unity value and the integral element gives the probability that the state variable x is beyond this acceptable short term maximum value, and, therefore, qualifies as a probability of failure. The term γ (gamma) gives the probability of malfunctioning of the protection system, i.e. the probability that the protection elements operate when there is no actual fault in the system, or the probability that a fault occurs in the system and the protection elements do not operate. That value is taken as a constant of 0.01.

$$P_t(x) = 1 - \int_0^{x_s} f_t(x)dx + \gamma \tag{4.4}$$

It is assumed that state variable x follows a truncated normal distribution $f_t(x)$ foe each interval Δt, with mean value x_{set}. The sensitivity factor α is introduced to characterize the relationship between mean value x_{set} and normal rating value x_n. Therefore, α is given by the ration between x_{set} and x_n. With the mean value defined, a third parameter β is introduced to determine the amount of dispersion of the normal distribution, and is given by equation 4.5, where δ is the variance of function $f_t(x)$. Parameter β is set to 5, while α is set to 1.3 for when state variable x represents current values, and 1.6 for when it represents voltage values.

$$\beta = \frac{x_S - x_n}{\delta} \tag{4.5}$$

For every period Δt, $P_t(x)$ will be determined both for x being considered the system's currents and the system's voltages. The following reliability analysis will be performed for the worst case or, the highest modeled failure rate, as expressed in equation 4.6.

$$\lambda = \max\{\lambda(\Delta U), \lambda(I)\} \tag{4.6}$$

Simulations

The modeling detailed in the last section aims to create a more realistic reliability analysis, in terms of the current value of the test system's state variables. Given that the load in a distribution system is constantly changing, as well as the power injection of the micro sources fluctuates between different hours of the day, it is reasonable to assume that the modeling results will be different according to the time of the day and the year, and that this will affect the reliability results. For that reason, the entire analysis was performed in an hour by hour basis, on a total of 8760 hourly analysis within a year, which is the reason for the interval Δt of one hour in equation 4.3.

For every one hour step, during an entire year, a different value of power demand will be used. Given that the IEEE test system only presents constant values of peak demand, it was necessary to obtain a yearly load profile. That information was taken from [23], whose measurements are taken from a residential area with peak demand of 10MW. This hour by hour load profile was used to scale the maximum load demand on each loadpoint

of the test system, allowing the simulations to translate changes throughout the year. The scaling coefficients taken from [23] are plotted in Figure 4.3.

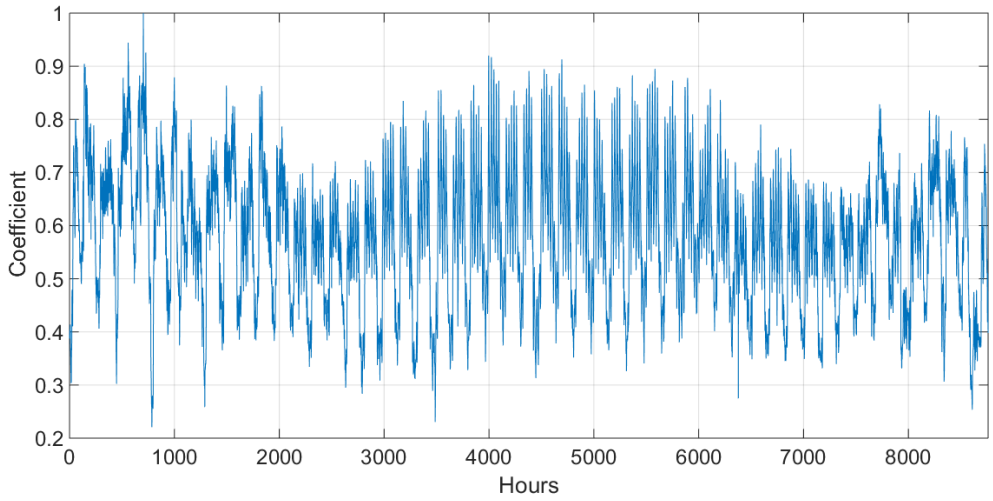

Figure 4.3 – Yearly load demand profile

Besides, for every one hour period, a different weather condition, i.e., a different value of wind speed, solar illuminance and temperature, must be considered. Both temperature and solar illuminance yearly profiles were obtained from measurements made by National Renewable Energy Laboratory, located in Oak Ridge, TN, throughout the year of 2014 [14]. For wind speed profile, the database of NASA's Modern-Era Retrospective Analysis for Research and Applications (MERRA) [24] was used. The information was related to the North Carolina area, more precisely to coordinates 34.5°N/-83°W, during the year of 2014. Figure 4.4 shows a plot for both illuminance (yellow curve) and wind speed (blue curve) profiles used. It is noticed from that figure that the illuminance profile is stronger during the middle months of the year, while wind is stronger during the earlier months, or the very latest ones.

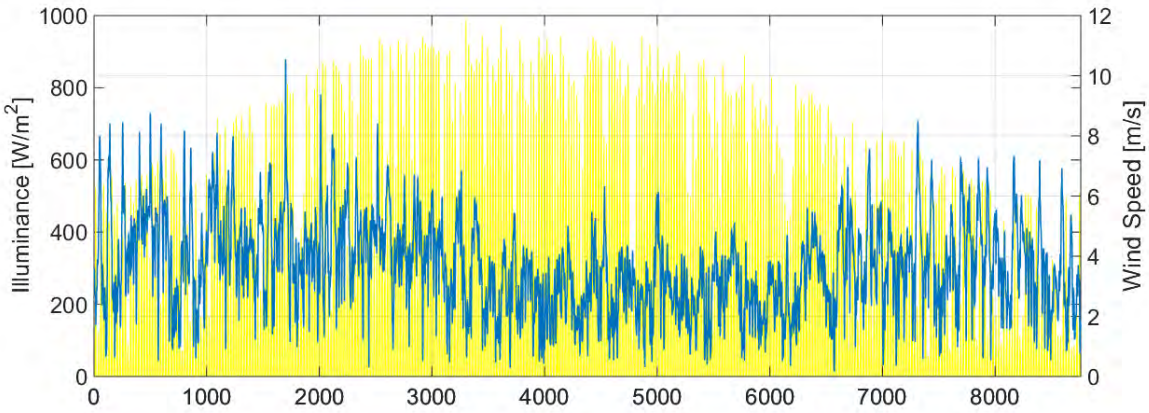

Figure 4.4 – Yearly profiles of solar illuminance and wind speed

Next, the state variables of the system are described through the Back/Forward Sweep power flow method, explained in section 4.1. With those results, the failure rate modeling from section 4.2 is performed and, finally, reliability indices are calculated. This process is then repeated to the next one hour period, for a total of 8760 calculations for the yearly analysis.

Given that power distribution systems are expected to be very reliable, their reliability indices are usually of small magnitude. For example, a SAIFI of 0.2 indicates that, on average, only one out of 5 customers will have any sort of interruption during a certain period of time, being that interruption of any duration. These indices are usually calculated for periods of one year, in order to assess the power utilities' service for that year. Since the analysis performed in this study is on hourly basis, it is to be expected that indices will be of a much smaller order.

Figures 4.5 through 4.11 show the resulting indices for the hour by hour analysis of each one of the 7 reliability indices presented in section 3.1. For each of those indices,

both the scenario with DG sources and without DG sources are being considered, so that the effects of micro source power injection can be evidenced. Notice how the format of the indices for the scenarios with failure rate modeling follows a shape similar to the load profile, shown in Figure 4.3, given that it is the increase in load demand that results in higher currents and voltage drops and, therefore, higher probability of having inadequate state variables. Also, in each of the figures, a constant line shows the result obtained through basic reliability analysis, considering only the standard failure rate λ_o.

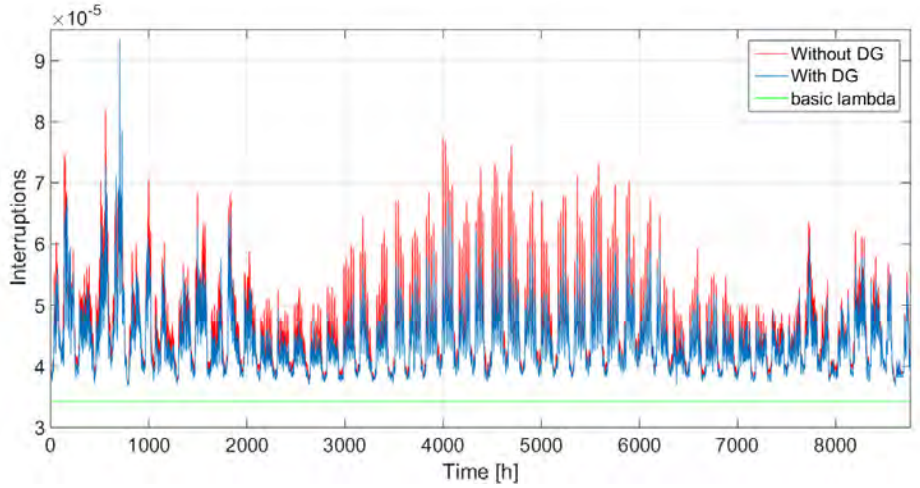

Figure 4.5 – Hourly SAIFI

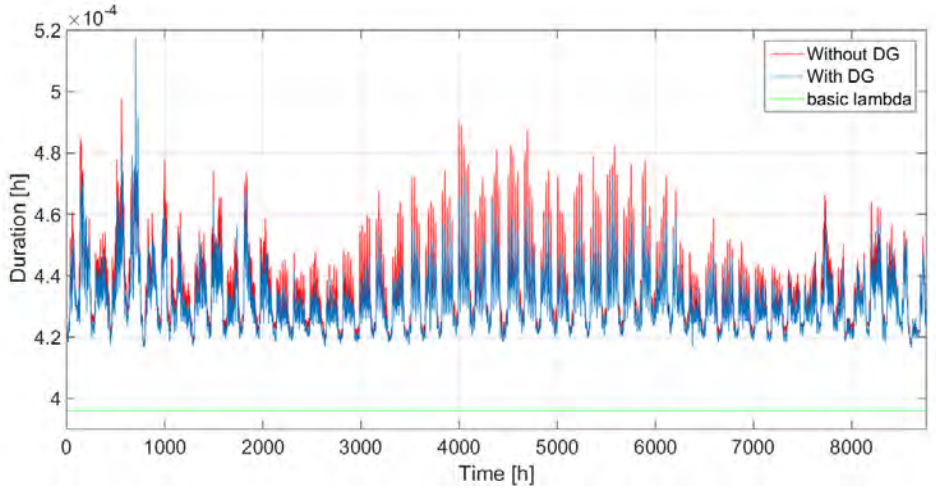

Figure 4.6 – Hourly SAIDI

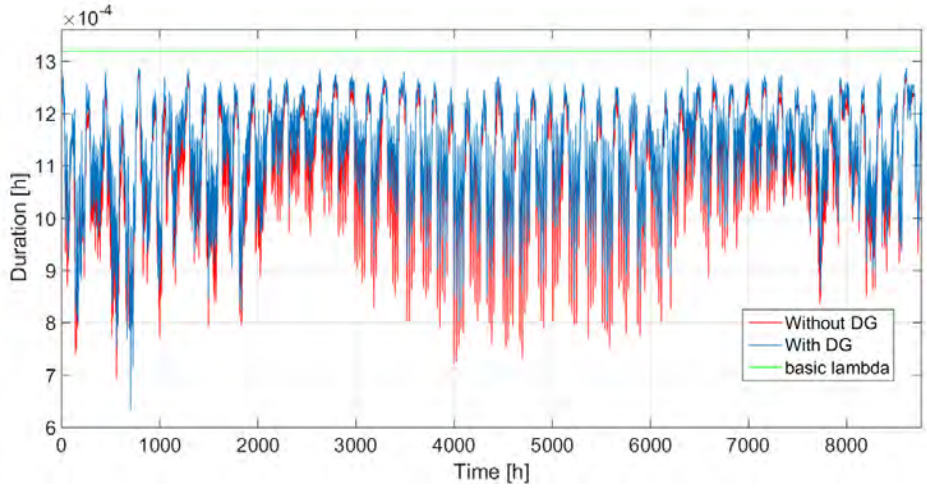

Figure 4.7 – Hourly CAIDI

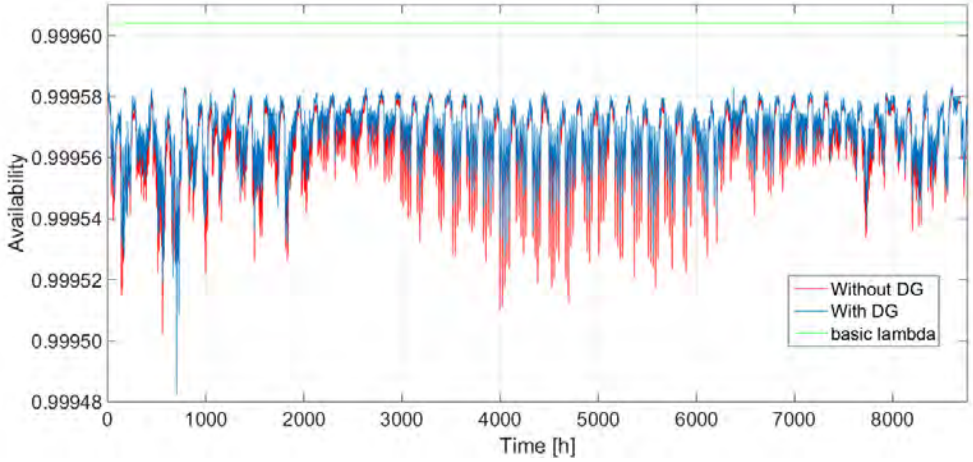

Figure 4.8 – Hourly ASAI

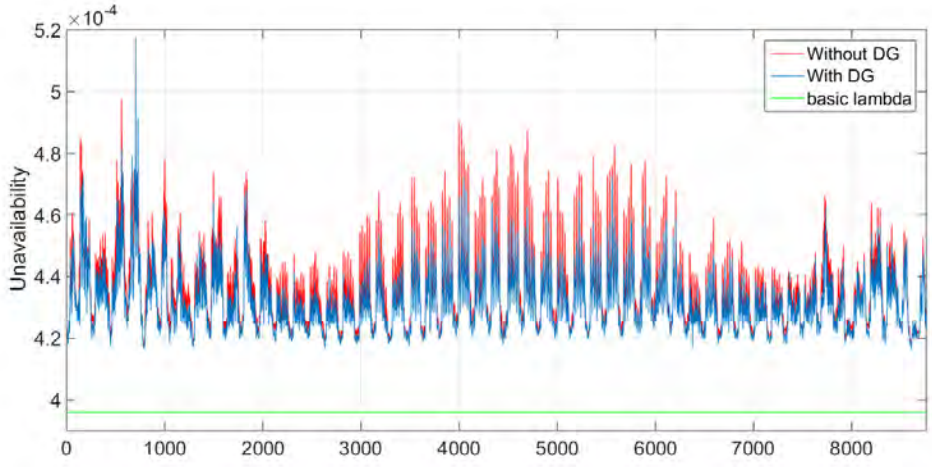

Figure 4.9 – Hourly ASUI

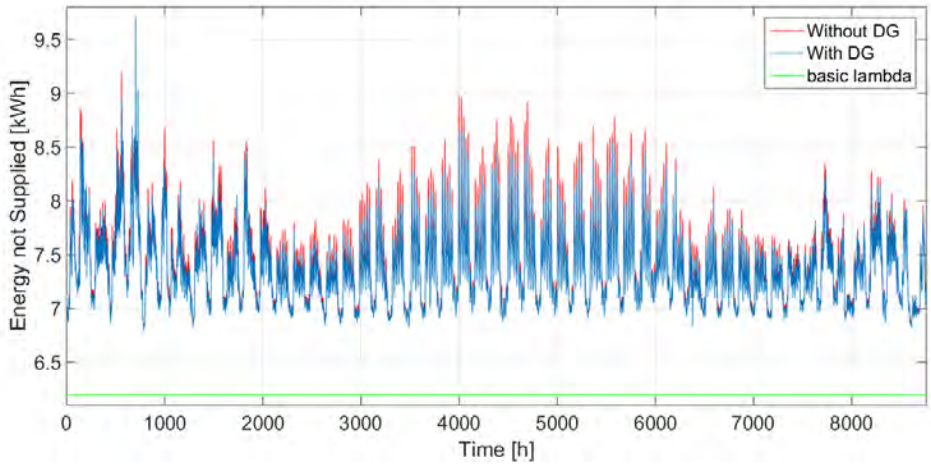

Figure 4.10 – Hourly ENS

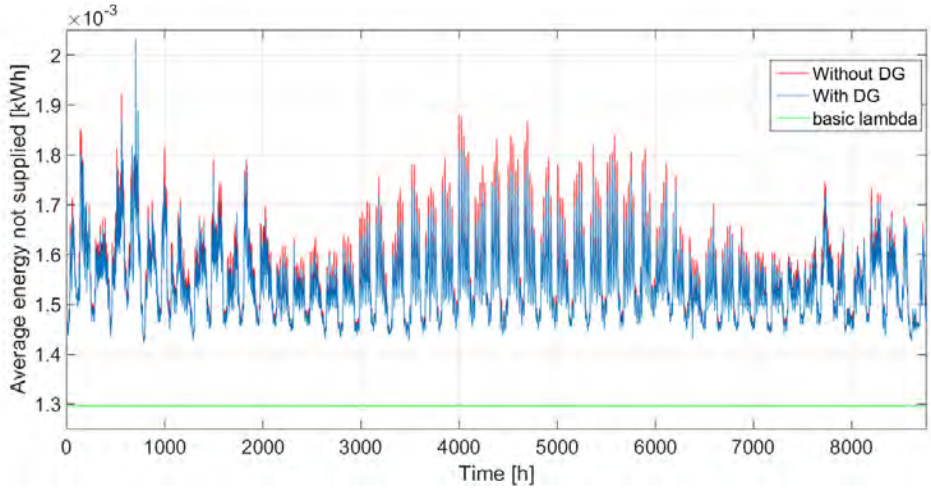

Figure 4.11 – Hourly AENS

From the figures above, it is possible to notice the effects of the failure rate modeling, as well as of the micro sources power injection, in the resulting reliability indices. Figures 4.5 and 4.6, for example, show that SAIFI and SAIDI were increased (worsened) when compared to the basic failure rate results represented by the green horizontal line, due to the Failure Rate Modeling. Once the probability of having inadequate state variable values is taken into consideration as a fault probability, the failure rate of the system is increased and the resulting indices are generally worsened. For the

case with DG, both indices are reduced (improved), when compared to the results without DG, and the reduction is more visible during the middle months of the year, when PV injection is at its highest. A similar behavior is seen for both the ENS and AENS indices, shown in figures 4.10 and 4.11, except the reduction in energy not supplied brought by the micro sources is more discrete than for the other two indices.

ASAI is shown, in figure 4.8, on the other hand, to be reduced (worsened) when compared to the basic failure rate case. This index translates the availability of the system. Due to the increase in failure rate, the system is expected to be less reliable, and less available. Once DG injection is considered, this index is slightly improved. Naturally, ASUI, shown in Figure 4.9 has the exact opposite behavior, given that this index translates the unavailability of the system.

Figure 4.7 shows the results for CAIDI. For this index, an improvement (reduction) is noticed when the state variables are considered into the failure rate modeling. That means that, on average, the interruptions in the system will have a shorter duration. This improvement is due to the fact that the increased failure rate is only considered for cable failure in the system. Other elements also have probability of failure, and for those, the outage time might be much larger, such as those of lateral transformers, whose outage time is of 200 hours [16]. In such case, the failure rate modeling will make it more likely that faults will happen in the cables, but not on the transformers, and since the cables have a smaller outage time, the CAIDI will be improved, despite the fact that the failure rate worsened all other indices.

Table 4.1 summarizes the indices for all three scenarios: first, the basic results, as presented in [16], in which the indices were calculated considering only basic failure rate are show as "reference". Second, the new set of indices calculated using the modeled failure rate, in which the system's state variables were being considered are shown in the two middle columns, with the percentual worsening of indices (with the exception of CAIDI, in which an improvement is seen, according to what was explained above). And lastly, the resulting indices from the scenario with failure rate modeling and distributed generation are presented in the last two columns, again with the percentual improvement relative to the scenario without DG. These indices are simply the resulting sum of all the 8760 results obtained for each hour of the year. The improvement with DG is relatively small, given that the weather conditions of the area are such that the DG sources are usually operating below maximum capacity, according to the equations on chapter 2.

	Reference	Failure Rate Modeling		With DG	
	Index	Index	Improvement [%]	Index	Improvement [%]
SAIFI	0.3	0.404	+ 34.67	0.385	- 4.70
SAIDI	3.47	3.82	+ 10.09	3.78	- 1.05
CAIDI	11.56	9.58	- 17.13	9.90	+ 3.34
ASAI	0.999604	0.999564	- 0.0040	0.999568	+ 0.0004
ASUI	3.96E-04	4.36E-04	+ 10.10	4.31E-04	- 1.15
ENS	54293	65068	+ 19.85	64626	- 0.68
AENS	11.36	13.62	+ 19.89	13.52	- 0.73

Table 4.1 – Summary of Indices

CHAPTER FIVE

STORAGE CONTRIBUTION

In power systems, even if steady state operation is being considered, there are small disturbances constantly happening, due to changes in load demand throughout the network. These disturbances must be matched by the generators, to assure that demand is constantly balanced by supply of generation. The correct functioning of the system, in terms of voltage levels, as well as frequency regulation, depends on this balance.

With the increasing penetration of renewable energy in the distribution grid, and the weather dependent characteristic of those sources, as was discussed in Chapter 2, the flexibility of the system operator to assure this demand-supply balance is compromised. Figure 5.1 shows the profile for solar irradiance, wind speed and load demand for different days through the year of 2014. This is the same data used for the analysis performed in Chapter 4, and the representation here is for the first day of each season of that year, i.e., March 20th as the first day of spring, June 20th as the first day of Summer, September 22nd as the first day of Fall, and December 21st as the first day of Winter. The data was scaled to 1 in order for all curves to be compared in the same curve, meaning that all values of load, wind speed and solar irradiance were divided by their respective annual maximum value.

From Figure 5.1, it is possible to see that the peak injection of the DG sources occur in different moments of the day, according to the season. For summer, and especially for winter, for example, one can see that this peak injection does not coincide with the peak system demand. Therefore, for the hours where the system is the most overloaded, the DG

sources are not participating as effectively as they could. For that reason, energy storage systems are usually introduced in order to better distribute the renewables power injection according to the load demand curve, and to provide further flexibility to the system.

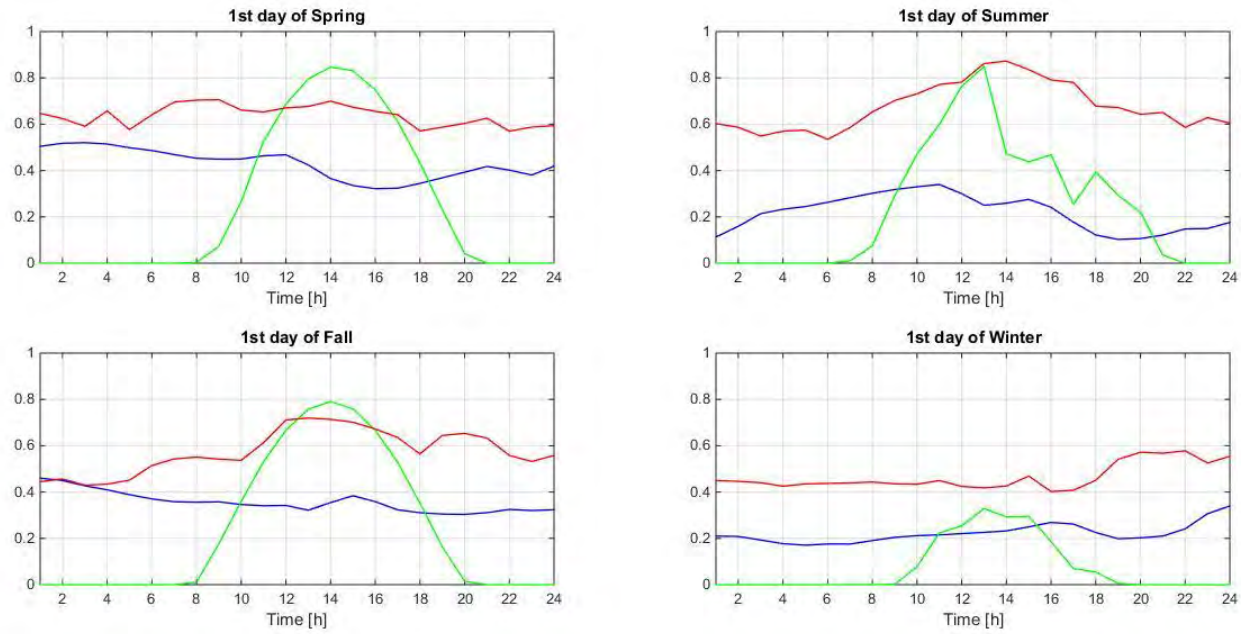

Figure 5.1 – Load demand, wind speed and solar irradiance profiles for each season

Besides, for higher load demands, the branches of the micro grid are subjected to a larger level of current. The modeling of failure rate according to voltage and current values, as presented in Chapter 4, is such that this would result in larger probability of failure and, therefore, decreased reliability. Storage systems may be employed to shave off this peak demand and avert this effect.

The goal of this chapter is to analyze the impacts of having storage systems within the micro grid, seeing if and by how much the reliability indices obtained in Chapter 4 are affected.

Battery Model

The degree of the detail of a battery model depend on the application to which it will be intended. The model must be reasonably accurate, yet manageable in terms of computational effort to the size of the system being studied.

Electric power and voltage supplied by a battery system have a shape similar to what is shown in Figure 5.2 [25]. In this figure, the battery voltage drops from its maximum, charged value, to zero, following a curve that can be divided into three sections: first, the discharge section, in which voltage drops quickly from maximum to nominal value. Second, a section that can be seen, in practice, as linear and with constant voltage and power injected, as the battery discharges. Lastly, the exponential area, in which the State of Charge (SOC) of the battery has dropped further enough that its stored power, as well as its supplied voltage exponentially drop to zero.

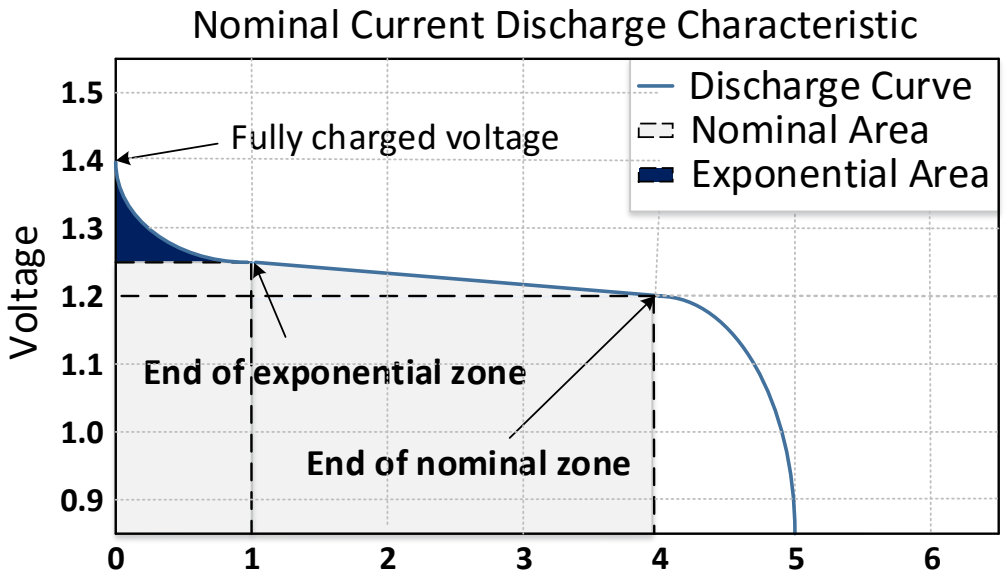

Figure 5.2 – Typical battery discharge profile

In practice, operation is limited to the nominal section, meaning that the SOC of the batteries are kept between 20% and 80% [26]. This is the consideration taken for the study presented in this chapter.

Other characteristics of battery systems may be taken into consideration, like the influence of temperature, and internal resistances. However, since this study is focused on reliability performance in steady state, a rather simple model of battery was adopted. Also, the storage capacity of a battery system drops along its life span. Since typical battery systems have life spans of the order of thousands of cycles [27], and given that in this yearly analysis the storage systems are not expected to go through a full discharge cycle more than once a day, it is expected that this effect won't be relevant through the first year of the study.

Simulation

Two battery systems were introduced into the IEEE 14-Bus test system, with capacities of 2MWh each. The initial assumption was that these systems would be connected to two out of the same four LPs that had the DG sources connected to. The choice of which DG sources would be paralleled with storage would be made based on the highest impact on reliability results. However, the improvement brought to the reliability indices with this placement was negligible. A new placement of the battery systems was then proposed, as is shown in Figure 5.3 below.

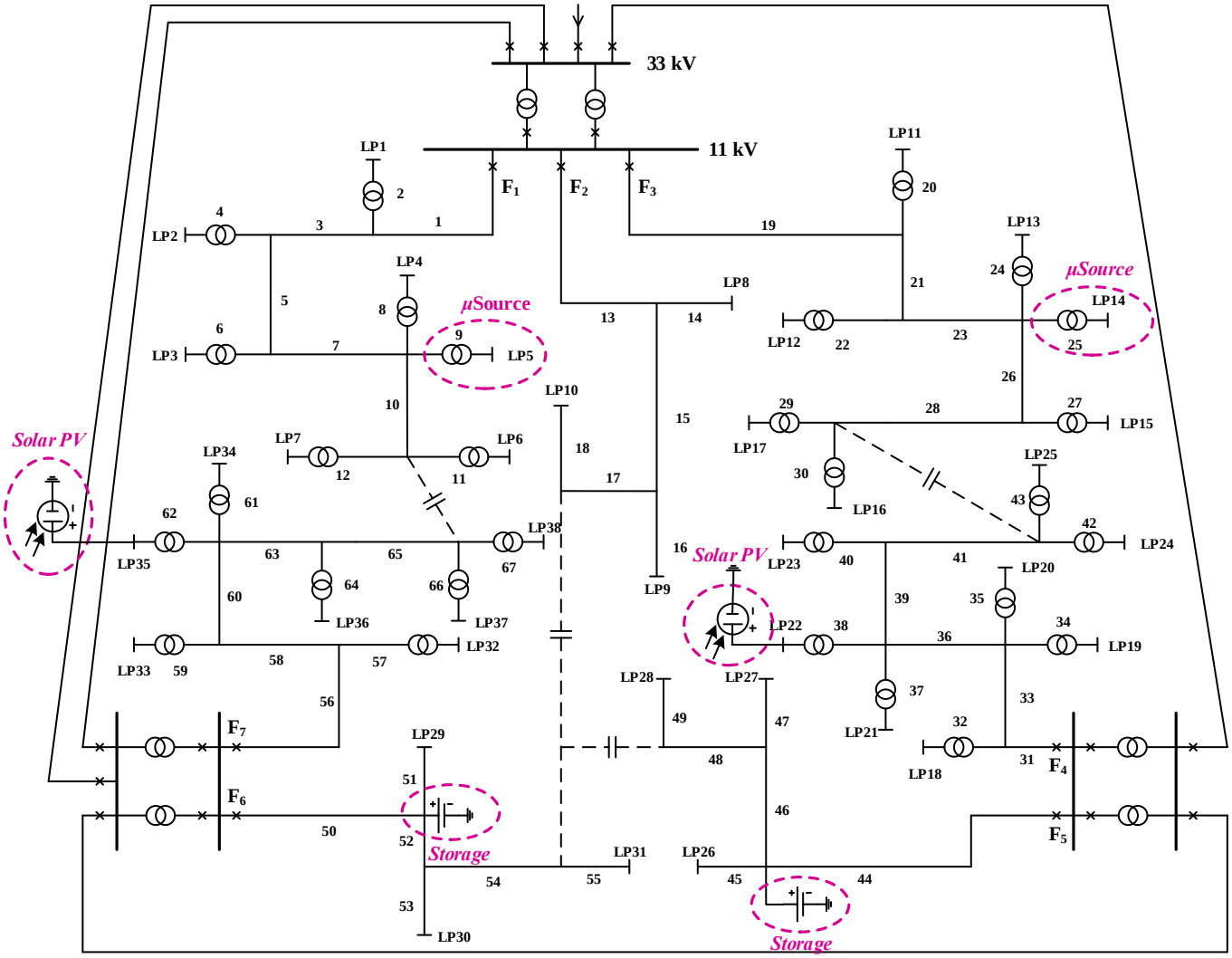

Figure 5.3 – Storage systems placement in the test system

With battery systems connected to nodes 44 and 50 of the test system, the yearly analysis performed in Chapter 4 was repeated, in order to quantify the impact brought by the storage systems. These systems were set in such a manner as to discharge at a constant rate during the hours of peak load. The power injection was of 300kW, and each system was capable of discharging over a period of 4 hours, with its SOC still remaining at the minimum established of 20%. The system would be recharged back to an 80% SOC over the remaining hours with less load, which is done at a slower rate than the rate of discharge. The charging demand for the batteries was set to 100kW.

The new set of reliability indices obtained from this analysis is shown in Table 5.1. The improvement on those results is also shown, as a comparison with the third scenario from Chapter 4, in which storage systems were not considered.

	Without Storage	With Storage	
	Index	Index	Improvement [%]
SAIFI	0.385	0.379	- 1.56
SAIDI	3.78	3.63	- 3.97
CAIDI	9.90	9.66	- 2.42
ASAI	0.999568	0.999585	+ 0.0017
ASUI	4.31E-04	4.14e-04	- 3.94
ENS	64626	61568	- 4.73
AENS	13.52	12.88	- 4.73

Table 5.1 – Storage contribution on reliability indices

Table 5.1 shows that all reliability indices were improved through the addition of the storage systems. Comparing these results with those on Table 4.1, we can see that the availability of the system (AENS, ENS, ASUI, ASAI) is improved in a more significant way than the improvement brought by the DG sources. Similarly, the average duration of the outages (SAIDI, and CAIDI) show larger improvement. The frequency of outages (SAIFI) was also improved, but in a more slightly manner than what was observed after the introduction of the DG sources.

The placement showed to be essential to maximize the positive impact of the battery systems in the microgrid. Through the reduction of currents in the network branches, the negative effects of failure rate model were mitigated. Also, having a new source of power within the grid means more flexibility in terms of rearranging the loads after a fault is detected, which reduces the average time of unavailability.

In this study, the microgrid is connected to a larger utility grid, which is considered to be entirely reliable. Only faults happening in the elements within it will harm its reliability. In practical systems, however, faults in the main grid might have the microgrid operating in islanded mode. In that case, the presence of DG sources, as well as battery systems plays an even more relevant role in maintaining power supply to as much load as possible. The decision to implement battery systems would, therefore, rely on an economic analysis of cost and benefits, depending on how reliable the system needs to be, and how sensitive, or critical, its customers are.

CHAPTER SIX

CONCLUSIONS AND FUTURE WORK

Utility companies are required to provide its customers with constant and reliable power supply. In case of faults or discontinuity, the system is expected to recover in as little time as possible, through the activation of the protection system, and losing the least amount of customers possible, through rearranging of loads. In engineering, an aspect such as reliability can't be treated as something subjective, and must be quantified. In order to do so, an analysis is performed onto the system and measured reliability indices are determined. Those different indices reflect reliability from different points of view, and are usually evaluated together for a more complete study.

Microgrid systems are smaller scale power distribution systems, including both loads and generation. The typical energy generation resources are renewable based, such as solar panels, wind turbines, and thermal power plants. These systems may operate connected to the main grid (on grid), or entirely independently (off grid). Microgrids have been playing a more important role in power systems and have been studied more deeply, due to its inherent advantages when compared to the more traditional model of power system, but also due to its higher complexity. This thesis aimed to investigate reliability of supply in microgrid systems.

The traditional analysis and calculation of reliability indices was explained in Chapter 3. The test system to which this analysis is applied was also presented in that same chapter. A different consideration to what is the base input of reliability analysis, the failure rate, is proposed in the beginning of Chapter 4, and was called Failure Rate Modelling. As

expected, the effects of such modelling were of a considerable worsening of the indices. The performed analysis presented in Chapters 4 and 5 were meant to quantify the changes in such indices. The initial analysis resulted in worsening of all indices, to a smaller or larger degree, with the exception of the CAIDI, for reasons explained in Chapter 4. The average impact on indices was of a worsening of 11.07% when Failure Rate Modeling was included. The conclusion drawn from this initial analysis was, therefore, that the traditional method or obtaining system elements failure rates leaves certain factor out of the picture, which can result in considerable overestimations of system reliability.

The second analysis conducted aimed to quantify the impacts brought by having DG sources within the microgrid. Four DG systems were introduced: two PV based systems of 2.0 and 2.5 MW of nominal power each, and two wind based systems, of 2.0 and 3.0 MW of nominal power each. The presence of power sources within the system, and closer to the loads reduced the power flow intensity, mitigating the negative effects brought by the Failure Rate Modeling. However, this positive impact was rather small, having an average improvement of 0.71% over all seven indices.

Given that the microgrid system was taken to be connected to an ideal infinity bus, no faults were being considered beyond the limits of the microgrid. Being that way, the contribution of the DG sources is limited, for their larger impact would occur for cases when the grid was not supplied by the main system, in a contingency scenario, and the loads, or at least the critical loads, had to be supplied only by the local generation. In those cases, the reliability indices would be deeply affected if no DG sources were present.

The last scenario simulated aimed to investigate the impacts brought by the presence of storage systems in the microgrid, which would be responsible for balancing the irregular power injection profile of the DG sources, caused by their weather dependent characteristics. Two battery systems were introduced, having storage capacity of 2MWh each. These systems had an average contribution of 3.05% in the indices. Similar to the DG sources, the storage systems might have even higher impact, if the possibility of fault in the main grid was being considered. For that case, a different logic of charge and discharge might need to be considered.

Future Work

In future expansions of this study, some more detailing can be obtained. First, the failure rate modeling only investigated the limitations imposed by standard onto the cables and nodes of the system. Distribution transformers were present in the microgrid, and were also possible faulted elements. The modeling of failure rate, however, did not consider the impact of the system's state variables to the transformers, and its failure rate was considered to be constant. The Failure Rate Modeling can be expanded to include the transformers.

Second, as was mentioned earlier, faults in the main grid were not being considered. A new and slightly more complete reliability analysis can be run, including the possibility of faults outside the microgrid, to which the system would respond by disconnecting itself and operating in off-grid mode. This would reduce the overall reliability of the system, but would better evidence the impacts of both the storage system and the DG sources.

The placement of the storage systems had been initially thought to coincide with the placement of the DG sources. However, placing these systems more towards the upstream nodes of the distribution feeders showed to have a better impact on the reliability indices. An optimal placement algorithm was not applied in this study and can be a valuable addition for the future.

APPENDIX

Appendix A

Matlab code for short term reliability index calculation

```
clear
clc
to=clock;
ref=1.0; % Ref Voltage
% Storage capacity is 2MWh. SOC allowed from 20% (400kWh) to 80%
(1600kWh). Initial value is at 80%
Capacity=2; Storage=0.8*Capacity;
n=68; b=67; % number of nodes (n) and branches (b)
% Base Power [MVA] Base Voltage [kV] Base Impedance [Ohms] Base Current
      Sb=10;           Ub=11;           Zb=Ub^2/Sb;     Ib=Sb*1000/Ub;

tamanho=8760; % Number of hours in a year. Creating variable Indices
SAIFI_System=zeros(tamanho,1);SAIDI_System=zeros(tamanho,1);
CAIDI_System=zeros(tamanho,1);ASAI_System=zeros(tamanho,1);
ASUI_System=zeros(tamanho,1);ENS_System=zeros(tamanho,1);
AENS_System=zeros(tamanho,1);

% Determining the power input of Microsources (Gs and Gw)
Wind_Data=load('Wind_NC_2014.txt');
Solar_Data=load('Solar_2014.txt');
Demand_Data=load('Load_and_coeff.txt');
Vci=2.5;Vrate=10;Vco=18; % Cut-in, Rated, and Cut-out speed, in m/s
Srate=1000;Erate=25; % Base Illuminance [W/m^2] and Rated temp [°C]

for loop=1:tamanho
% ------------------- Wind ----------------------------------------
WindSpeed=Wind_Data(loop,1);
 if WindSpeed<Vco
  if WindSpeed>Vrate
    Gw=1; % Full power for larger than Vrate speeds
  elseif WindSpeed>Vci
    Gw=(WindSpeed-Vci)/(Vrate-Vci); % Fluctuant power for medium speeds
  else
    Gw=0; % No power for both too high speeds
  end
  else
    Gw=0; % Or too low speeds
 end
% ----------------- Solar ----------------------------------------
Illuminance=Solar_Data(loop,3);Temperature=Solar_Data(loop,4);
nfactor=1-0.0045*(Temperature-Erate);
Gs=(Illuminance/Srate)*nfactor;
% ----------- Determine whether or not DG is considered -------------
DGInd = 1; % If DGInd==1, DG is being considered.
% Assuming first two DG sources are wind, and two others are PV based.
% 1st: Injection node; 2nd: Injected power
DG=[ 9 Gw*3/Sb;25 Gw*2/Sb;38 Gs*2.5/Sb;62 Gs*2/Sb];
```

```
        if DGInd == 0 % If zero, microsources are not being considered
            DG(:,2) = 0; % All injected power is zero
        end
       %------------------------- System Analysis --------------------------
       % 1st: 1 branch #; 2nd: From Node; 3rd: To node; 4th: Impedance [pu];
       % 5th: Load demand [pu]; 6th: DG power injection');
Z=
[1 0 1 (0.099+0.2685i)/Zb 0/Sb -0/Sb; 2 1 2 (0.378+0.2208i)/Zb 0.545/Sb -0/Sb;
 3 1 3 (0.1056+0.2864i)/Zb 0/Sb -0/Sb;4 3 4 (0.4725+0.276i)/Zb 0.545/Sb -0/Sb;
 5 3 5 (0.1056+0.2864i)/Zb 0/Sb -0/Sb;6 5 6 (0.378+0.2208i)/Zb 0.545/Sb -0/Sb;
 7 5 7 (0.2025+0.25125i)/Zb 0/Sb -0/Sb;8 7 8 (0.504+0.2944i)/Zb 0.545/Sb-0/Sb;
 9 7 9 (0.4725+0.276i)/Zb 0.5/Sb -0/Sb;10 7 10 (0.162+0.201i)/Zb 0/Sb -0/Sb;
11 10 11 (0.504+0.2944i)/Zb 0.415/Sb -0/Sb;12 10 12 (0.4725+0.276i)/Zb 0.415/Sb -0/Sb;
13 0 13 (0.1056+0.2864i)/Zb 0/Sb -0/Sb;14 13 14 (0.378+0.2208i)/Zb 1/Sb -0/Sb;
15 13 15 (0.1056+0.2864i)/Zb 0/Sb -0/Sb;16 15 16 (0.4725+0.276i)/Zb 1.5/Sb -0/Sb;
17 15 17 (0.162+0.201i)/Zb 0/Sb -0/Sb;18 17 18 (0.504+0.2944i)/Zb 1/Sb -0/Sb;
19 0  19 (0.099+0.2685i)/Zb 0/Sb -0/Sb;20 19 20 (0.504+0.2944i)/Zb 0.545/Sb -0/Sb;
21 19 21 (0.0792+0.2148i)/Zb 0/Sb -0/Sb;22 21 22 (0.4725+0.276i)/Zb 0.545/Sb -0/Sb;
23 21 23 (0.1056+0.2864i)/Zb 0/Sb -0/Sb;24 23 24 (0.4725+0.276i)/Zb 0.545/Sb -0/Sb;
25 23 25 (0.378+0.2208i)/Zb 0.5/Sb -0/Sb;26 23 26 (0.216+0.268i)/Zb 0/Sb -0/Sb;
27 26 27 (0.4725+0.276i)/Zb 0.5/Sb -0/Sb;28  26  28  (0.162+0.201i)/Zb 0/Sb -0/Sb;
29 28 29 (0.4725+0.276i)/Zb 0.415/Sb -0/Sb;30 28 30 (0.378+0.2208i)/Zb 0.415/Sb -0/Sb;
31 0  31 (0.1056+0.2864i)/Zb 0/Sb -0/Sb;32 31 32 (0.4725+0.276i)/Zb 0.545/Sb -0/Sb;
33 31 33 (0.1056+0.2864i)/Zb 0/Sb -0/Sb;34 33 34 (0.378+0.2208i)/Zb 0.545/Sb -0/Sb;
35 33 35 (0.4725+0.276i)/Zb 0.545/Sb -0/Sb;36 33 36 (0.1056+0.2864i)/Zb 0/Sb -0/Sb;
37 36 37 (0.4725+0.276i)/Zb 0.545/Sb -0/Sb;38 36 38 (0.378+0.2208i)/Zb 0.5/Sb -0/Sb;
39 36 39 (0.216+0.268i)/Zb 0/Sb -0/Sb;40 39 40 (0.4725+0.276i)/Zb 0.5/Sb -0/Sb;
41 39 41 (0.162+0.201i)/Zb 0/Sb -0/Sb;42 41 42 (0.4725+0.276i)/Zb 0.415/Sb -0/Sb;
43 41 43 (0.378+0.2208i)/Zb 0.415/Sb -0/Sb;44 0 44 (0.1056+0.2864i)/Zb 0/Sb -0/Sb;
45 44 45 (0.4725+0.276i)/Zb 1/Sb -0/Sb;46 44 46 (0.0792+0.2148i)/Zb 0/Sb -0/Sb;
47 46 47 (0.504+0.2944i)/Zb 1/Sb -0/Sb;48 46 48 (0.2025+0.25125i)/Zb 0/Sb -0/Sb;
49 48 49 (0.378+0.2208i)/Zb 1/Sb -0/Sb;50 0  50 (0.099+0.2685i)/Zb 0/Sb -0/Sb;
51 50 51 (0.378+0.2208i)/Zb 1/Sb -0/Sb;52 50 52 (0.1056+0.2864i)/Zb 0/Sb -0/Sb;
53 52 53 (0.4725+0.276i)/Zb 1/Sb -0/Sb;54 52 54 (0.216+0.268i)/Zb 0/Sb -0/Sb;
55 54 55 (0.378+0.2208i)/Zb 1.5/Sb -0/Sb;56 0 56 (0.099+0.2685i)/Zb 0/Sb -0/Sb;
57 56 57 (0.504+0.2944i)/Zb 0.545/Sb -0/Sb;58 56 58 (0.0792+0.2148i)/Zb 0/Sb -0/Sb;
59 58 59 (0.504+0.2944i)/Zb 0.545/Sb -0/Sb;60 58 60 (0.099+0.2685i)/Zb 0/Sb -0/Sb;
61 60 61 (0.378+0.2208i)/Zb 0.545/Sb -0/Sb;62 60 62 (0.504+0.2944i)/Zb 0.545/Sb -0/Sb;
63 60 63 (0.2025+0.25125i)/Zb 0/Sb -0/Sb;64 63 64 (0.378+0.2208i)/Zb 0.5/Sb -0/Sb;
65 63 65 (0.2025+0.25125i)/Zb 0/Sb -0/Sb;66 65 66 (0.504+0.2944i)/Zb 0.5/Sb -0/Sb;
67 65 67 (0.378+0.2208i)/Zb 0.415/Sb -0/Sb];  % Q is considered to be zero

       % ------------------------ Load Demand -------------------------------
       LoadDemand=Demand_Data(loop,2); % 'LoadDemand' will store the coeff
                                       % (0-1) for nominal demand of each LP
       for m=1:size(Z,1)
         Z(m,5)=Z(m,5)*LoadDemand*2;
       end
       % ----------------- Battery power injection/demand ------------------
           temp=fix((loop-1)/24); % How many days have passed
           day=Demand_Data(temp*24+1:temp*24+24,2);
           day=sort(day,'descend');
           power=0;
```

```
    if LoadDemand<day(12,1) % 12 hours of lowest demand, battery charge
        power=0.1; % Positive power = Battery charging
        if Storage+power>0.8*Capacity
            power=0.8*Capacity-Storage;
            Storage=0.8*Capacity; % 80% max charge
        else
            Storage=Storage+power;
        end
    elseif LoadDemand>day(5,1) % 4h of max demand, battery discharges
        power=-0.3; % Negative power = Battery discharging
        if  Storage+power<0.2*Capacity
            power=0.2*Capacity-Storage;
            Storage=0.2*Capacity; % 20% min charge
        else
            Storage=Storage+power;
        end
    end
% Inclusion of variable power into certain nodes
power=power/Sb;Z(9,5)=Z(9,5)+power; Z(25,5)=Z(25,5)+power;
% Inclusion of DG power injection into Z matrix (Column 6)
  for m=1:1:size(DG,1) % For each node that has microsource injection
    for k=1:1:size(Z,1)
      if Z(k,1)==DG(m,1)
       Z(k,6)=-DG(m,2);
      end
    end
  end
    % Adition of Feeder# for each branch to matrix Z (Column 7)
NewCol=zeros(size(Z,1),1);
Z=[Z,NewCol]; % Addition of 7th columns to Z, referring to Feeder#
 x=0; % Feeder counting
  for k=1:1:size(Z,1) % Sweeping of all branches (all rows of Z)
    if Z(k,2)==0 % If zero, means a new branch starts
       x=x+1;
    end
       Z(k,7)=x; % 7th column of Z has feeder numbers of each branch
  end
   faultedfinal=0;

% ------- Application of Back/Forward Sweep Method (Power Flow)--------
error=1; % enters the while loop
V1=ones(n,1); % Initial guess of voltages
while error>0.001
 I=zeros(size(Z,1),1); % Initial value of currents
   for k=1:1:size(Z,1)
      if Z(k,5)~=0 % For power diferent than zero - Final node
       I(k,1)= conj((Z(k,5)+Z(k,6))/V1(k+1,1));
      end
   end
for k=size(Z,1):-1:1
 for m=size(Z,1):-1:1
     if Z(k,3)==Z(m,2)
       I(k)=I(k)+I(m,1); % Branch k has current of final node
     end
```

```
 end
end

% Calculating new set of voltages from the obtained currents
 V2=ones(n,1)*ref;.
 for k=1:1:size(Z,1) % For each branch
     V2(Z(k,3)+1,1)=V2(Z(k,2)+1,1)-I(k)*Z(k,4);
 end
     V2(faulted+1,1)=V2(faulted,1);
 end
  error=V1-V2;
  V1=V2;
 End
% Voltage magnitudes and angles in the same matrix
Vm=abs(V1);theta=angle(V1);Voltages=[Vm theta];

% ---------------------- Failure Rate modeling ------------------------
% Matrix In has the maximum ampacity current of all sections
In=[610;220;610;220;610;220;380;220;220;380;220;220;610;220;610;220;
380;220;610;220;610;220;610;220;220;380;220;380;220;220;610;220;610;
220;220;610;220;220;380;220;380;220;220;610;220;610;220;380;220;610;
220;610;220;380;220;610;220;610;220;610;220;220;380;220;380;220;220];
% Simulation values taken from reference
alphaI=1.3; alphaU=1.6; beta=5; gama=0.001;
% Calculating Pi
 In=In/Ib;Is=In*1.7;
 DeltaI=(Is-In)/beta; % Variance
 SigmaI=sqrt(DeltaI); % Standard deviation
 Iset=alphaI*I; % Mean Value
 Pi=1-normcdf(Is,Iset,SigmaI)+gama;
% Calculating Pu
 VoltDeviation=abs(Voltages(2:end,1)-ones(67,1))*100;
 Un=5;Us=10; % Max deviation
 DeltaU=(Us-Un)/beta; % Variation
 SigmaU=sqrt(DeltaU); % Standard deviation
 Uset=alphaU*VoltDeviation; % Mean Value
 Pu=1-normcdf(5*ones(67,1),Uset,SigmaU)+gama;
% Determining Px, as max(Pu,Pi)
 Px=zeros(67,1);
 for m=1:size(Pi,1)
   Px(m,1)=max(Pi(m,1),Pu(m,1))+0.065;
 end

% ----------------- Reliability Analysis (System Indices)-------------
repair=5; % Repair time of each Section or lateral Distributor [hours]
lambdaT=0.015; % Failure rate of the distribution transformers
repairT=200; % Down time of transformers
% Adition of branch length on matrix Z (Column 8)
NewCol=[0.75;0.6;0.8;0.75;0.8;0.6;0.75;0.8;0.75;0.6;0.8;0.75;0.8;0.6;
0.8;0.75;0.6;0.8;0.75;0.8;0.6;0.75;0.8;0.75;0.6;0.8;0.75;0.6;0.75;0.6;
0.8;0.75;0.8;0.6;0.75;0.8;0.75;0.6;0.8;0.75;0.6;0.75;0.6;0.8;0.75;0.6;
0.8;0.75;0.6;0.75;0.6;0.8;0.75;0.8;0.6;0.75;0.8;0.6;0.8;0.75;0.6;0.8;
0.75;0.6;0.75;0.8;0.6]; Z=[Z,NewCol];
```

```
 for k=1:size(NewCol,1
   NewCol(k,1)=NewCol(k,1)*Px(k,1); % Failure rates
 end
Z=[Z,NewCol]; % Failure rates [failure/year] added to Z
% Unavailability [hour/year] added to Z
NewCol=zeros(size(Z,1),1);Z=[Z,NewCol];
 for k=1:size(Z,1)
   if Z(k,5)==0 % No load in k - section of main feeder. No load
     Z(k,10)=Z(k,9)*0.5; % 0.5h of unavailability for all LPs in feeder
   else % If branch is final branch
     Z(k,10)=Z(k,9)*5; % Unavailability of 5h for that one specific LP
% Feeders 2,5 and 6 are supplied in 11kV and have no transformers. For
all others, we must add the failure rate of transformers.
  if Z(k,7)~=2 && Z(k,7)~=5 && Z(k,7)~=6
     Z(k,9)=Z(k,9)+lambdaT;Z(k,10)=Z(k,10)+lambdaT*repairT;
  end
  end
 end
% Load characteristics
% 1: LP#, 2: Feeder#, 3: # of customers, 4th: Avg. Load demand [kW]
LP=[1 1 220 545;2 1 220 545 ;3 1 220 545 ;4 1 220 545 ;5 1 200 500;
    6 1 10  415;7 1 10 415  ;8 2 1 1000  ;9 2 1 1500  ;10 2 1 1000;
   11 3 220 545;12 3 220 545;13 3 220 545;14 3 200 500;15 3 200 500;
   16 3 10 415; 17 3 10 415 ;18 4 220 545;19 4 220 545;20 4 220 545;
   21 4 220 545;22 4 200 500;23 4 200 500;24 4 10 415; 25 4 10 415;
   26 5 1 1000; 27 5 1 1000; 28 5 1 1000; 29 6 1 1000; 30 6 1 1000;
   31 6 1 1500; 32 7 220 545;33 7 220 545;34 7 220 545;35 7 220 545;
   36 7 200 500;37 7 200 500;38 7 10 415];
NewCol=zeros(size(LP,1),2);
LP=[LP,NewCol];LPnumber=0; % First new column (5th) is total failure
% rate for every LP. Second (6th) is total U [hours/year] for every LP
for k=1:size(Z,1)
  if Z(k,5)~=0
     LPnumber=LPnumber+1;
     LP(LPnumber,5)=Z(k,9);
     LP(LPnumber,6)=Z(k,10);
       for m=1:size(Z,1)
         if Z(m,5)==0 && Z(m,7)==Z(k,7)
            if Z(m,3)==Z(k,2)
              LP(LPnumber,5)=LP(LPnumber,5)+Z(m,9);
              LP(LPnumber,6)=LP(LPnumber,6)+10*Z(m,10);
            else
              LP(LPnumber,5)=LP(LPnumber,5)+Z(m,9);
              LP(LPnumber,6)=LP(LPnumber,6)+Z(m,10);
            end
            end
        end
      end
 end

 % These results will give us the following:
numberofcustomers=0;  numberofinterruptions=0;
interruptionduration=0; energynotsupplied=0;
```

```
for m=1:size(LP,1)
 numberofcustomers=numberofcustomers+LP(m,3);
 numberofinterruptions=numberofinterruptions+LP(m,5)*LP(m,3);
% Product of lambda of a certain LP and its number of customers
 interruptionduration=interruptionduration+LP(m,6)*LP(m,3);
% Product of unavailability of a certain LP and its number of customers
 energynotsupplied=energynotsupplied+LP(m,6)*LP(m,4);
end

% Calculating the reliability indices for the whole system
SAIFI_System(loop,1)=numberofinterruptions/numberofcustomers;
SAIDI_System(loop,1)=interruptionduration/numberofcustomers;
CAIDI_System(loop,1)=interruptionduration/numberofinterruptions;
ASAI_System(loop,1)=(numberofcustomers*8760-
interruptionduration)/(numberofcustomers*8760);
ASUI_System(loop,1)=1-ASAI_System(loop,1);
ENS_System(loop,1)=energynotsupplied;
 AENS_System(loop,1)=energynotsupplied/numberofcustomers;
End

% We divide all vectors of reliability indices by 8760. That's why it
was not necessary to consider a smaller failure rate for the failure
rate modeling part. If we weren't making this division now, we would
have had to consider failure rate of 0.065/8760
SAIFI_System=SAIFI_System/8760;SAIDI_System=SAIDI_System/8760;
CAIDI_System=CAIDI_System/8760;ASAI_System=ASAI_System/8760;
ASUI_System=ASUI_System/8760;ENS_System=ENS_System/8760;
AENS_System=AENS_System/8760;

% Adding them all for final yearly results
SAIFI_Final=sum(SAIFI_System);SAIDI_Final=sum(SAIDI_System);
CAIDI_Final=sum(CAIDI_System);ASAI_Final=sum(ASAI_System);
ASUI_Final=sum(ASUI_System);ENS_Final=sum(ENS_System);
AENS_Final=sum(AENS_System);

fprintf('\nSAIFI:\n');display(SAIFI_Final);
fprintf('\nSAIDI:\n');display(SAIDI_Final);
fprintf('\nCAIDI:\n');display(CAIDI_Final);
fprintf('\nASAI:\n');display(ASAI_Final);
fprintf('\nASUI:\n');display(ASUI_Final);
fprintf('\nENS:\n');display(ENS_Final);
fprintf('\nAENS:\n');display(AENS_Final);

% Displays the total time taken by the simulation
total_time=etime(clock,to)
```

REFERENCES

[1] B. S. Hartono, Budiyanto, and R. Setiabudy, “Review of microgrid technology,” *2013 Int. Conf. Qual. Res. QiR 2013 - Conjunction with ICCS 2013 2nd Int. Conf. Civ. Sp.*, pp. 127–132, 2013.

[2] R. Billinton, *Reliability Evaluation of Power Systems*, Second Edi. 1996.

[3] X. Xu, J. Mitra, T. Wang, and L. Mu, “Evaluation of operational reliability of a microgrid using a short-term outage model,” *IEEE Trans. Power Syst.*, vol. 29, no. 5, pp. 2238–2247, 2014.

[4] K. Balasubramaniam, R. Hadidi, and E. Makram, “Optimal operation of microgrids under conditions of uncertainty,” *2015 IEEE Power Energy Soc. Gen. Meet.*, pp. 1–5, 2015.

[5] O. Kaplan, U. Yavanoglu, and F. Issi, “Country study on renewable energy sources in Turkey,” *2012 Int. Conf. Renew. Energy Res. Appl.*, pp. 1–5, 2012.

[6] M. S. Celiktas, T. Sevgili, and G. Kocar, “A snapshot of renewable energy research in Turkey,” *Renew. Energy*, vol. 34, no. 6, pp. 1479–1486, 2009.

[7] T. Seba, *Clean Disruption of Energy and Transportation*, EBook Edit. 2014.

[8] M. I. B. V. Silva, “Estudo E Desenvolvimento De Um Sistema Eólico De Pequeno Porte Para Interligação À Rede Elétrica,” 2010.

[9] “Upper Great Plains Wind Energy Programmatic EIS.” [Online]. Available:

http://www.plainswindeis.anl.gov/guide/basics/index.cfm.

[10] NOAA, “US Wind Climatology,” 2015. [Online]. Available: https://www.ncdc.noaa.gov/societal-impacts/wind/.

[11] W. Underground, “Weather History - Clemson, SC,” 2015. [Online]. Available: http://www.wunderground.com/.

[12] A. G. Cook, L. Billman, and R. Adcock, “Photovoltaic Fundamentals,” *J. Plast. Surg. Hand Surg.*, vol. 48, no. 1, p. 96, 2014.

[13] T. Dhaka, “Modelling of Solar Cell Characteristics Considering the Effect of Electrical and Environmental Parameters,” pp. 9–14, 2015.

[14] Oak Ridge National Laboratory, “Weather Measurements,” 2015. [Online]. Available: http://www.nrel.gov/midc/ornl_rsr/.

[15] C. ISO, “What the duck curve tells us about managing a green grid,” *Calif. ISO, Shap. a Renewed Futur.*, vol. Fact Sheet, pp. 1–4, 2012.

[16] R. N. Allan, R. Billinton, I. Sjarief, L. Goel, and K. S. So, “A Reliability Test System for Educational Purposes - Basic Distribution-System Data and Results,” *Ieee Trans. Power Syst.*, vol. 6, no. 2, pp. 813–820, 1991.

[17] R. Singh, G. Alapatt, and G. Bedi, “Why and how photovoltaics will provide cheapest electricity in the 21st century,” *Facta Univ. - Ser. Electron. Energ.*, vol. 27, no. 2, pp. 275–298, 2014.

[18] J. Grainger and W. Stevenson, *Power System Analysis*, First. 1994.

[19] G. Andersson, "Modelling and Analysis of Electric Power Systems," *EEH - Power Syst. Lab.*, no. September, p. 183, 2008.

[20] S. Ghosh and D. Das, "Method for load-flow solution of radial distribution networks," *IEE Proc. - Gener. Transm. Distrib.*, vol. 146, no. 6, p. 641, 1999.

[21] E. June, "Power Quality Standards for Electric," pp. 1–15, 2009.

[22] W. Brogan, *Modern Control Theory*, Third Edit. 1990.

[23] D. Energy, "Duke Energy SCADA Historian," no. April, 2014.

[24] NASA, "MERRA," 2015. [Online]. Available: http://gmao.gsfc.nasa.gov/research/merra/.

[25] O. Tremblay, L. -a. Dessaint, and a.-I. Dekkiche, "A Generic Battery Model for the Dynamic Simulation of Hybrid Electric Vehicles," *2007 IEEE Veh. Power Propuls. Conf.*, no. V, pp. 284–289, 2007.

[26] J. A. Chahwan, *Vanadium-redox flow and lithium-ion battery modelling and performance in wind energy applications*, no. May. 2007.

[27] G. Huff, A. B. Currier, B. C. Kaun, D. M. Rastler, S. B. Chen, D. T. Bradshaw, and W. D. Gauntlett, "DOE/EPRI 2013 electricity storage handbook in collaboration with NRECA," *Rep. SAND2013- ...*, no. July, p. 340, 2013.